# GLOBAL SIMULATIONS OF BOUNDARY-LAYER CLOUDINESS: SENSITIVITY TO FORMULATION

David A. Randall
Laboratory for Atmospheres, NASA/Goddard Space Flight Center,
Greenbelt, Maryland

## 1. INTRODUCTION

Boundary-layer clouds are among the most important cloud types for both climate and weather. Low clouds produce a net radiative cooling of both the atmosphere and the earth's surface, thus potentially influencing the stability of the climate system. They create hazards for aviation and surface transportation, very effectively screen out the sun, and tend to discourage outdoor recreation.

Unfortunately, they are notoriously difficult to forecast or simulate with general circulation models. In many cases, model results show an excessive global abundance of boundary-layer clouds, but with simulated local cloudiness minima where local maxima are observed to occur.

Recently, Suarez et al. (1983) have described a parameterization of PBL stratocumulus clouds that has been incorporated into the UCLA GCM. Randall et al. (1985) have presented an analysis of the climate simulated by this model, with particular attention to the simulated PBL stratocumulus clouds.

In the present paper, we first summarize and then extend the results of Randall et al. (1985); in particular, we present preliminary results obtained with a new radiation parameterization.

## 2. MODEL DESCRIPTION

Results will be presented from a 9-level version of the GCM, which has its top at 50 mb. The prognostic variables of the model are the potential temperature, the mixing ratio of water vapor, the horizontal wind components, the surface pressure, the PBL depth, and the ground temperature and snow

depth at land and seaice points. The governing equations are finite-differenced, using highly conservative schemes (Arakawa and Lamb, 1977, 1981; Arakawa and Suarez, 1983). The mass flux and pressure gradient vectors are Fourier-filtered to maintain computational stability near the poles. For the simulations discussed in this paper, the horizontal resolution used was 5 degrees of longitude by 4 degrees of latitude. The time-steps used were 7.5 minutes for the dynamics and 1 hour for the physical parameterizations.

The prescribed boundary conditions include realistic topography, an idealized distribution of surface roughness, and the observed climatological seasonally varying global distributions of sea-surface temperature, sea ice, surface albedo, and ground wetness.

The GCM employs a modified sigma coordinate, in which the PBL top is a coordinate surface, and the PBL itself is the lowest model layer. As already mentioned, the PBL depth is a prognostic variable of the model. The mass sources and sinks for the PBL consist of large-scale convergence or divergence, turbulent entrainment, and the cumulus mass flux. Turbulent entrainment is driven by positive buoyancy fluxes, and/or by shear production at the surface and PBL top (Randall, 1979, 1984a). The surface fluxes are determined by the method of Deardorff (1972). The cumulus mass flux and the warming and drying of the free atmosphere due to cumulus convection are determined through the cumulus parameterization of Arakawa and Schubert (1974), as implemented by Lord et al. (1982).

For the baseline run described in this paper, we used the solar and terrestrial radiation parameterizations described in detail by Schlesinger (1976). The solar radiation parameterization includes both the diurnal and seasonal cycles. The terrestrial radiation parameterization includes cooling due to water vapor, carbon dioxide, and ozone. Cloudiness can occur in any

model layer, and can be associated with large-scale saturation, PBL stratocumulus clouds, or the anvils of deep cumuli. When and where cloudiness occurs, it is assumed to fill the entire horizontal extent of a grid box, for simplicity.

Stratocumulus clouds are assumed to be present in the PBL whenever the temperature and mixing ratio at the PBL top (as determined by a mixed-layer assumption) correspond to supersaturation, provided that the cloud-top entrainment stability criterion of Randall (1980a) is met. The cloud base is determined as the level at which the saturation mixing ratio is exactly equal to the mixing ratio of water vapor, using the mixed-layer assumption. Thus the simulated stratocumulus clouds can be arbitrarily thin, or they can fill the PBL. The presence of the stratocumulus clouds is felt by the GCM through both the radiation and turbulent entrainment parameterizations. The latter takes into account the generation of turbulence kinetic energy through increased buoyancy fluxes associated with cloud-top radiative cooling and phase changes (Randall 1980a, 1980b, 1984a). As a result of these cloud-enhanced buoyancy fluxes, the presence of a stratocumulus layer in the PBL tends to favor more rapid entrainment and, therefore, a deeper PBL.

When the PBL top is supersaturated but the cloud-top entrainment stability criterion is <u>not</u> met, the PBL is assumed to exchange mass with the free atmosphere. The amount of mass exchanged is that required to remove the supersaturation, or to restore stability, whichever is less. In most cases, supersaturation is removed, and the cloudiness is then set to zero for the radiation calculation. The PBL depth is assumed to remain unchanged during this mixing process, which we call "layer cloud instability" (LCI). As discussed by Randall (1984b), this parameterization of LCI is very crude, but results presented in Section 4.1 show that it improves the GCM's simulation of low cloudiness.

Details of the model description are given by Suarez et al. (1983), Randall et al. (1985), and references therein.

## 3. SUMMARY OF BASELINE RESULTS

In this Section, we briefly summarize January and July results presented by Randall et al. (1985), who analyzed a 37-month simulation, which was started from a December 31 initial condition taken from an earlier long run with a different version of the model. Most of the results presented are based on composites of the second, third, and fourth Januarys of the run, and the first, second, and third Julys.

As discussed by Randall et al. (1985), the model's simulation of the seasonally varying tropospheric circulation is generally satisfactory. The simulated sea-level pressure and 200 mb height patterns are very realistic. The simulated surface air temperature and surface winds are in good agreement with observations, although the surface humidity is lower than observed. The simulated polar winter upper troposphere is colder than observed, and the simulated upper tropospheric westerlies are correspondingly too strong. The simulated mean meridional circulation is weaker than observed. The simulated tropical middle troposphere is too dry, and the midlatitude upper troposphere is too humid. The geographical distribution of precipitation is realistic, although the predicted values appear to be somewhat too large. Since the model's water budget balances, the simulated evaporation is also somewhat too strong.

The simulated global distributions of the PBL depth, for January and July, are shown in Fig. 1. For both months, the time-averaged PBL depth is generally smaller over land than over the sea, because over land there is a strong contribution from the shallow nocturnal PBL, while over the sea the diurnal variability of the PBL depth is small. The seasonal changes

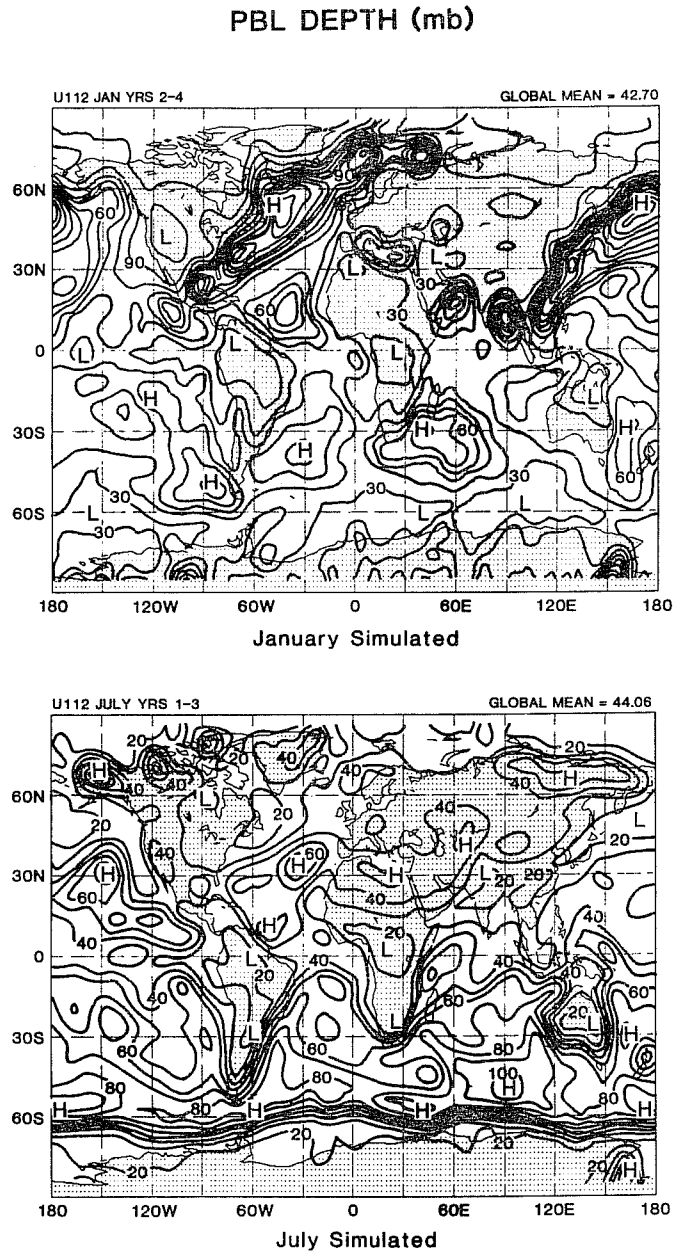


Figure 1. Simulated monthly mean maps of the PBL depth, in mb, for January and July. The contour interval is 10 mb.

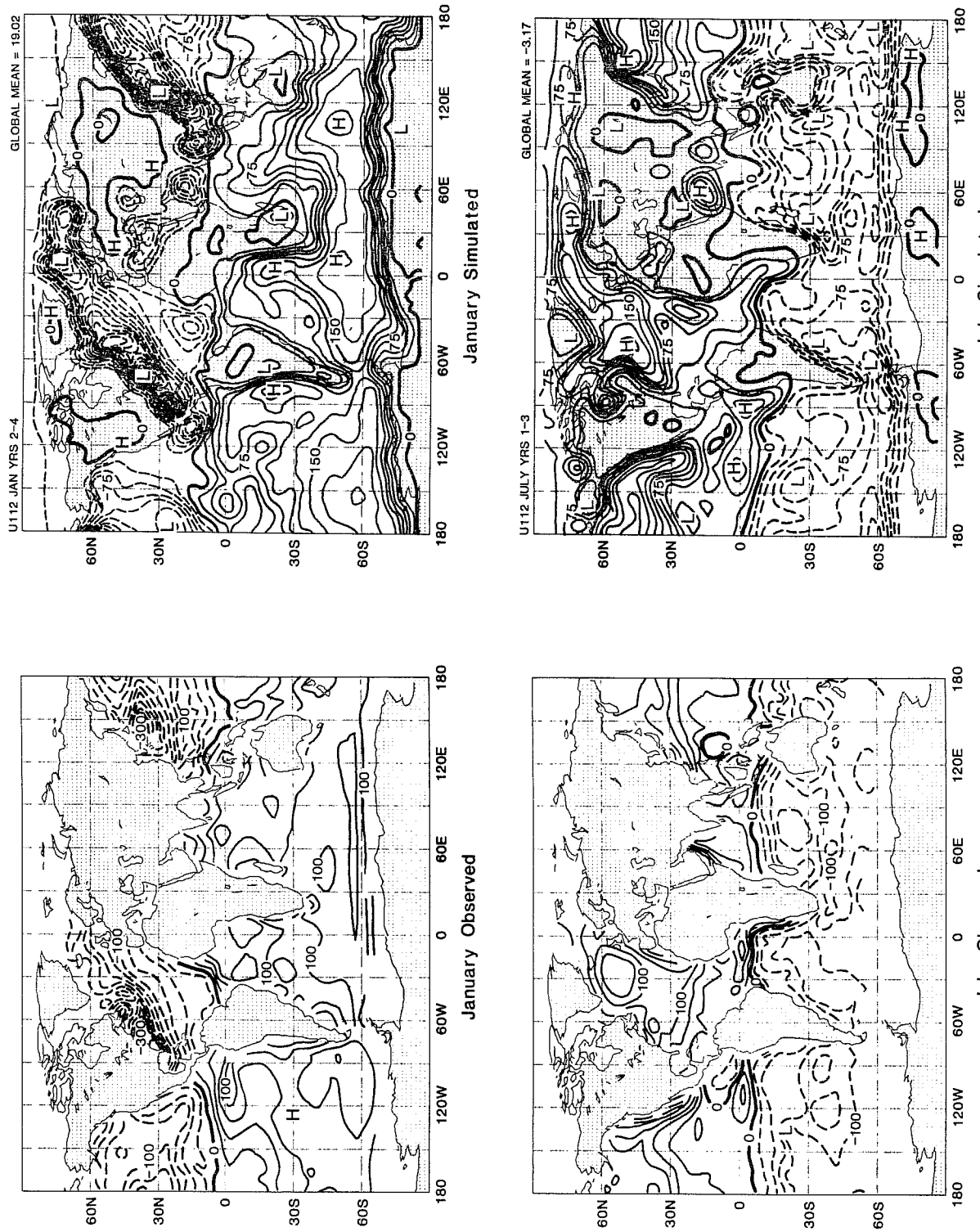


Figure 2. Simulated and observed (Esbensen and Kushnir, 1981) total surface energy flux, for January and July. The observations are plotted only for the oceans. The contour interval is 25 W $m^{-2}$. The zero contour is heavy, and negative contours are dashed.

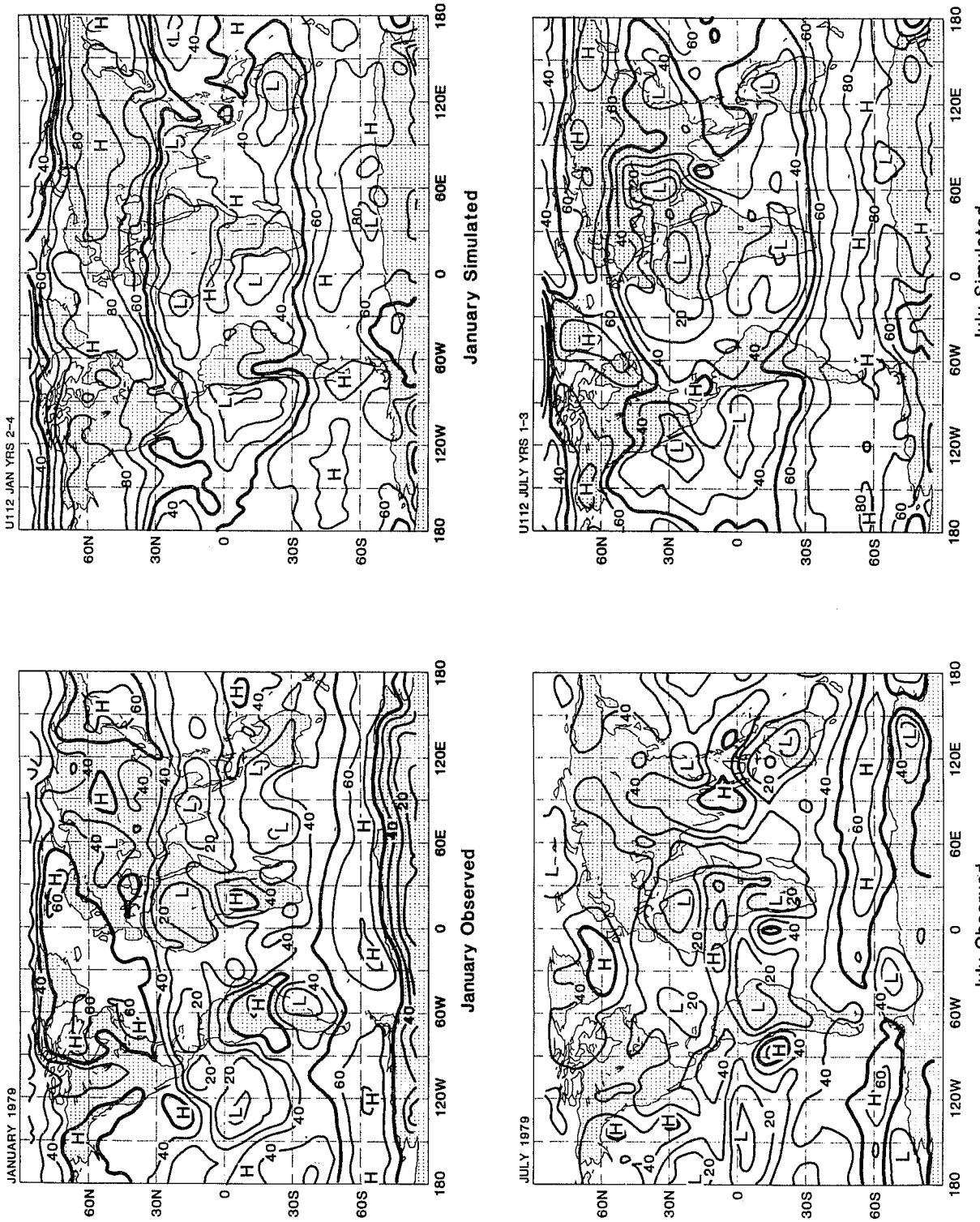


Figure 3. Simulated and observed monthly mean maps of total cloudiness, in %. The observations are based on the work of Susskind et al. (1984). The contour interval is 10%, and the 50% contour is heavy.

in the PBL depth pattern are very dramatic. For January, prominent maxima are found over the Gulf Stream and Kuroshio, in the regions of cold-air outbreaks over the warm sea. January maxima also occur over the Mediteranean and the Bay of Bengal. For July all of these maxima have disappeared. Instead, we find a deep PBL over the sea near Antarctica, where surface heating and strong surface westerlies maintain vigorous PBL turbulence. July maxima of the PBL depth also occur over the subtropical oceans. As discussed later, these are associated with PBL stratocumulus clouds.

The simulated and observed January and July distributions of the total downward surface energy flux (net downward solar radiation minus net upward longwave radiation minus upward turbulent latent heat flux minus upward turbulent sensible heat flux) are shown in Fig. 2. The observations are based on the data of Esbensen and Kushnir (1981) for the world oceans. The model sucessfully simulates the observed large upward heat fluxes over the Kuroshio and Gulf Stream in January, and over the Antarctic Circumpolar current in July. Over most of the tropical and subtropical oceans, the surface virtual temperature flux is upward, in agreement with observations, but the surface sensible heat flux is downward.

Fig. 3 shows the observed (Susskind et al., 1984) and simulated total cloudiness patterns, for January and July. The simulated globally averaged total cloudiness is near 50%; and the simulated planetary albedo is 30% for January and 28% for July, consistent with observations (e.g., Stephens et al., 1981). The model has a tendency to overpredict cloudiness in high latitudes, and to underpredict it in the tropics. In general, however, the simulated geographical and seasonal variations of the total cloudiness are fairly realistic, with maxima in the tropics and in midlatitudes, particularly in the winter hemisphere. The midlatitude maxima of the northern winter are strongest over the Gulf Stream and Kuroshio, in agreement with observations.

However, the observed minima over central Canada and central Asia are not simulated. For July, the model produces realistic maxima near Greenland, and in the region of the Indian monsoon. The simulated cloudiness associated with the July ITCZ is less prominent than observed, even though the tropical rain belt is very well simulated. This suggests that the GCM underpredicts tropical cirrus cloudiness, perhaps because the cloud matter detrained from deep cumulus clouds is not allowed to persist in the model. The subtropical marine stratocumulus regimes are discernable in the simulated total cloudiness maps, but they are much more conspicuous in the observations.

Figs. 4 and 5 show the simulated January and July distributions of stratocumulus incidence and stratocumulus depth, respectively. Comparison of the simulated stratus incidence results with the data of London (1957) and Hahn et al. (1982) shows reasonable agreement. The simulated globally averaged stratus incidence is in the range 12-15%, consistent with the data of London (1957), but lower than the values given by Hahn et al. (1982). In the January simulation, thin stratocumulus sheets occur with excessive frequency over the northern continents. This contributes to the excessive total cloudiness over central Canada and central Asia (cf. Fig. 3). However, because the simulated clouds in these regions are so very thin (~ 10 mb), the excessive simulated cloudiness may not be a serious deficiency.

Simulated January maxima of stratocumulus incidence and depth occur over the Gulf Stream and Kuroshio, in qualitative agreement with observations (Chou and Atlas, 1981; Ninomiya and Akiyama, 1976). Detailed inspection of the model results shows that in these reigons the PBL stratocumulus clouds tend to be associated with cold-air outbreaks. Simulated January maxima of stratocumulus incidence and depth occur off the subtropical west coasts

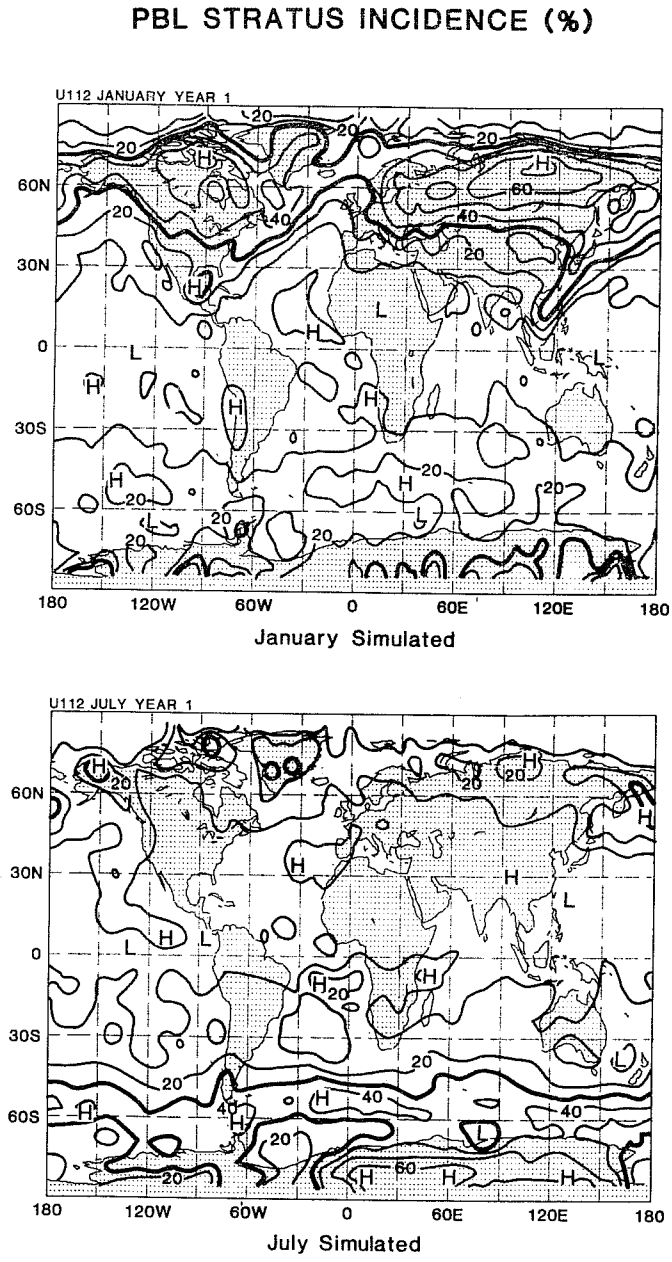


Figure 4. Simulated monthly mean maps of the simulated PBL stratus incidence, in %, for January and July. The contour interval is 10%, and the 30% contour is heavy.

PBL STRATUS DEPTH (mb)

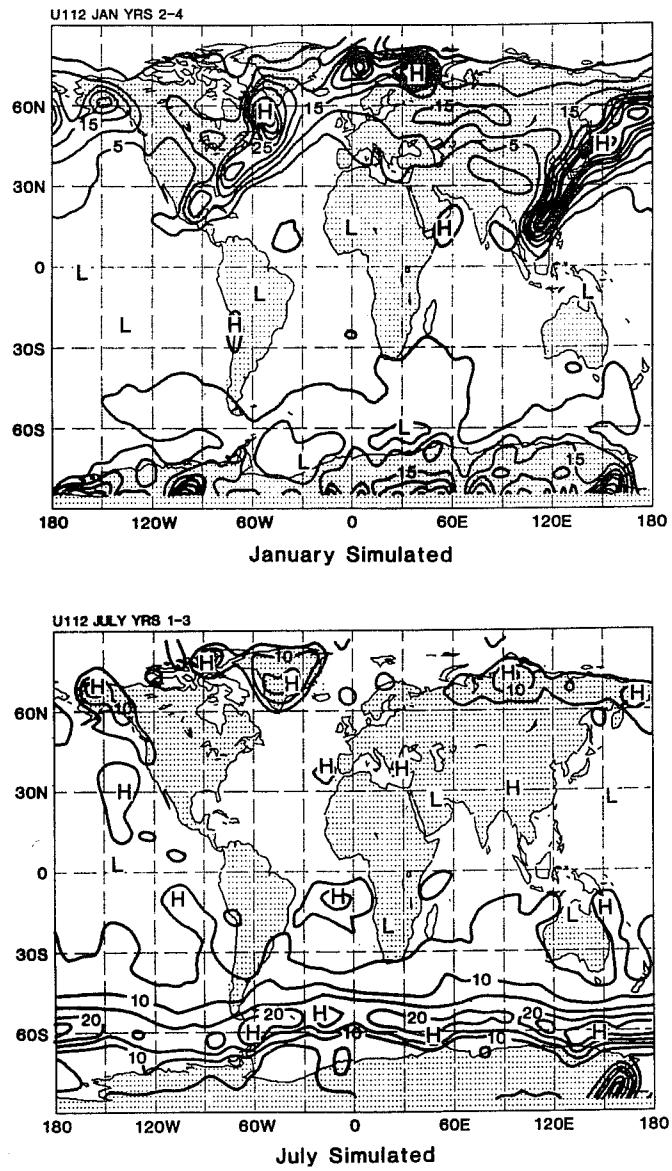


Figure 5. Simulated monthly mean maps of the simulated PBL stratus depth, in mb, for January and July. The contour interval is 5 mb.

of South America, southern Africa, and Australia, in agreement with observations. Similarly, simulated July maxima of stratocumulus incidence and depth are clearly evident off the subtropical west coasts of North America, South America, Europe, southern Africa, and Australia. The positions of these maxima are realistic (e.g., Neiburger et al., 1961; Miller and Feddes, 1971; Berliand and Strokina, 1980), but the simulated clouds do not occur as frequently as observed. As a result, marine subtropical stratocumulus clouds cause only slight maxima in the simulated total cloudiness (cf. Fig. 3). They are associated with maxima in the simulated PBL depth (cf. Fig. 1); for the July results, the spatial correlation of the monthly means of the stratus incidence and PBL depth is 0.64 over the oceans.

The GCM barely produces a hint of the observed summertime abundance of Arctic stratus (Huschke, 1969; Vowinckel and Orvig, 1970; Herman and Goody, 1976; Crane and Barry, 1984). The only partial success is that in the model results, as in the real atmosphere, the most prominent Arctic maximum of stratus incidence occurs near 150° W longitude, over the sea north of Alaska. Although we are unsure of the reason for the model's failure to simulate abundant summer Arctic status cloudiness, it appears that the prescribed seaice albedoes (0.70, independent of wavelength) are probably too high; lower sea ice albedoes would lead to increased evaporation and, possibly, more low clouds. A second contributing factor is that the GCM does not take into account the existence of open water in the summer ice pack. The presence of open water tends to increase the surface evaporation rate, and so favors the formation of low-level clouds.

For the continents, the GCM produces simulated stratocumulus clouds more often at night than during the day. As an example, Fig. 6 shows the July-mean diurnal cycle of stratocumulus incidence for the second year of the run, composited by local time, for 28 North American grid points. The diurnal

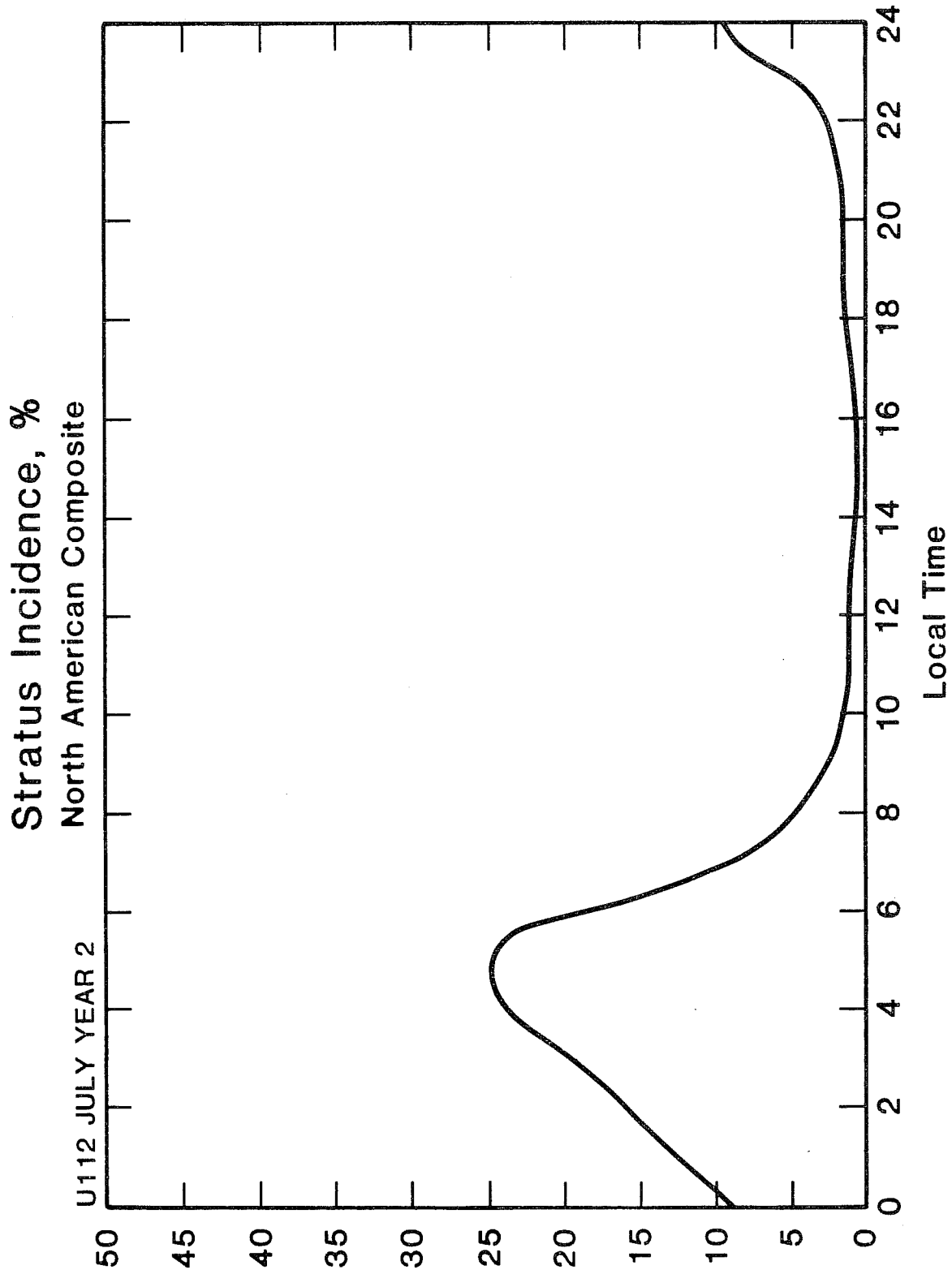


Figure 6. Simulated diurnal variation of stratocumulus incidence, composited by local time, for the North American grid points indicated in Fig. 1, and for July of the second simulated year.

variability of low cloudiness over land, which seems to be qualitatively well simulated by the model, can significantly modulate the land-surface energy balance. The potential importance of this fact has long been recognized (e.g., Brooks, 1927). During the daylight hours, low clouds reduce the solar radiation incident at the earth's surface. At any time of day, they reduce the net outgoing terrestrial radiation at the surface. Therefore, a tendency for low clouds to occur primarily at night over land increases the net input of radiative energy to the land surface, relative to the energy input that would occur if the same cloudiness were distributed uniformly over all hours of the day and night. Moreover, because low clouds have little effect on the outgoing terrestrial radiation at the top of the atmosphere, but a potentially large effect on the planetary albedo, a tendency for them to occur primarily at night minimizes their effect on the radiation budget of the earth-atmosphere system. Further discussion is given in Section 4c. The model does not simulate the observed diurnal variability of low cloudiness over the oceans (Neiburger et al., 1961; Kraus, 1963; Short and Wallace, 1980). This may be due to our failure to account for the effects of solar warming on entrainment.

Fig. 7 shows the simulated cooling of the PBL by terrestrial radiation, for January and July. The cooling is heavily concentrated over land, especially over high terrain, and it appears to be unrealistically weak over the oceans. There is no evident correspondence between cooling maxima and stratus incidence maxima. The simulated January and July solar warming of the PBL is shown in Fig. 8. The warming is naturally weakest in the winter hemisphere. The January results are relatively featureless, but there is a strong July maximum on the Tibetan Plateau. There are also July maxima of about 0.7 K $day^{-1}$ in the subtropical marine stratocumulus regimes of the Northern Hemisphere.

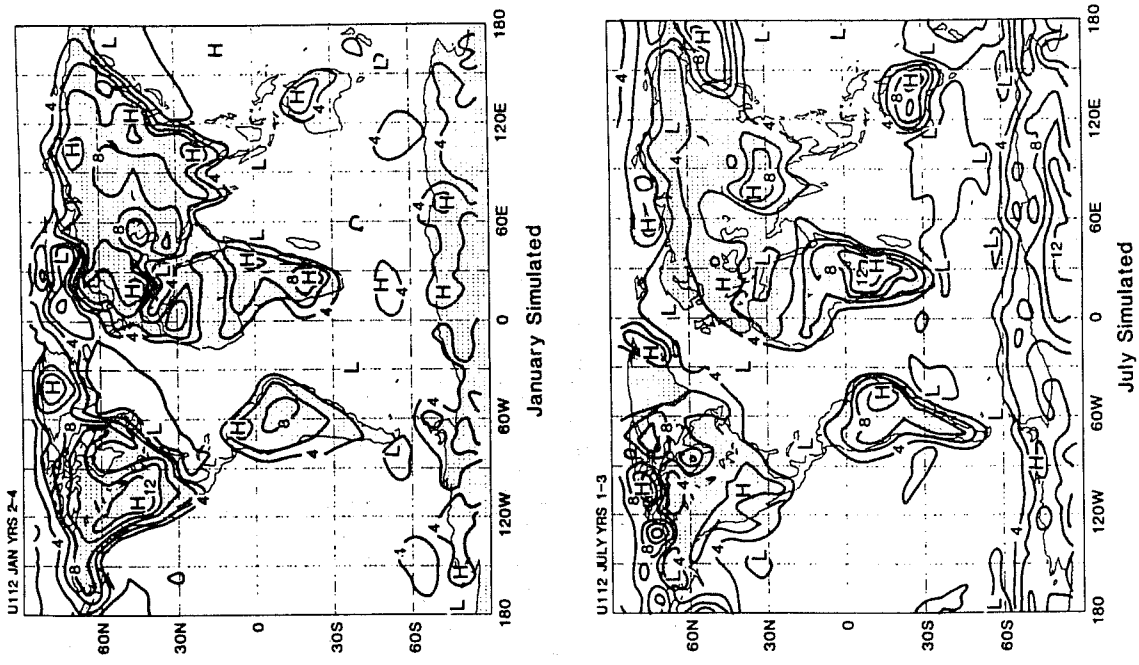


Figure 7. Simulated cooling of the PBL by terrestrial radiation, in K day$^{-1}$. The contour interval is 2 K day$^{-1}$.

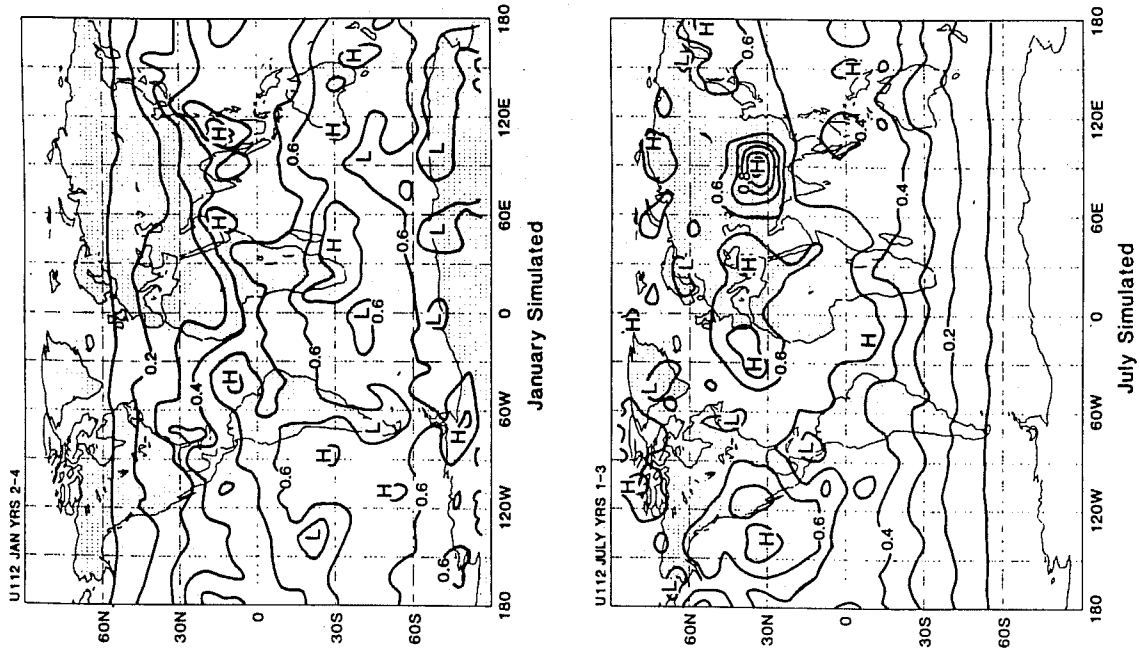


Figure 8. Simulated warming of the PBL by solar radiation, in K day$^{-1}$. The contour interval is 0.1 K day$^{-1}$.

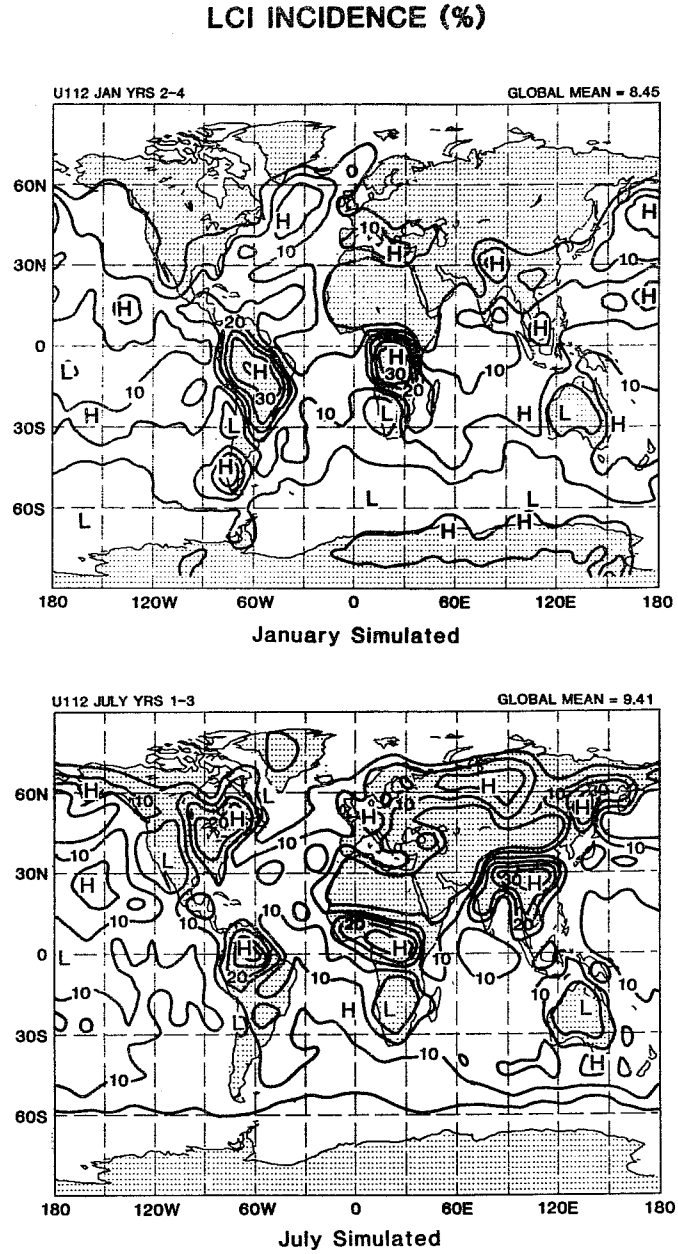


Figure 9. Monthly mean maps of the simulated frequency of ocurrence of LCI, the layer cloud instability, in %. The contour interval is 5%.

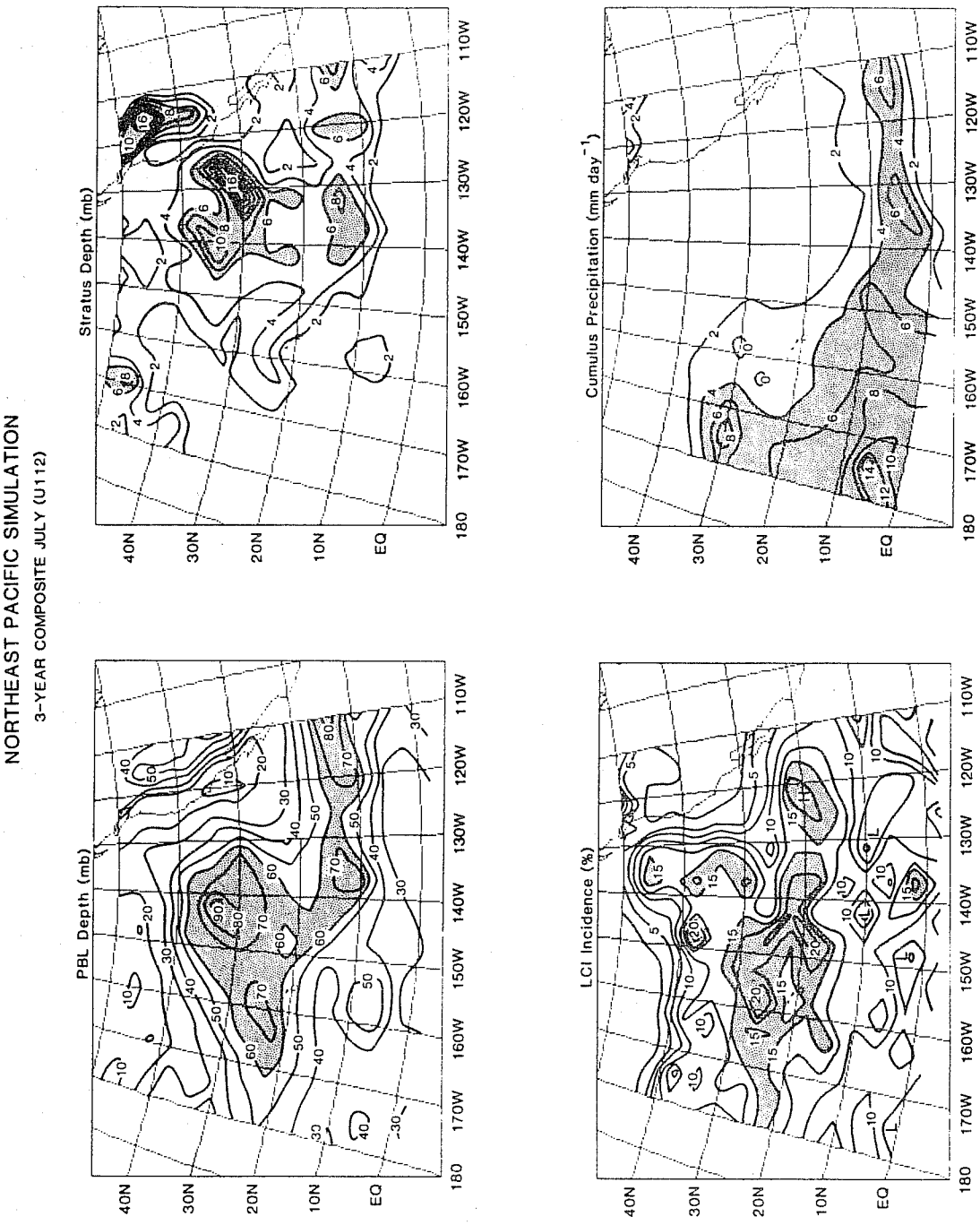


Figure 10. Regional maps of the simulated July-mean PBL depth (top left, contour interval 10 mb, values greater than 60 mb shaded), PBL stratus depth (top right, contour inverval 2 mb, values greater than 6 mb shaded), LCI incidence (bottom left, contour interval 5%, values greater than 15% shaded) and cumulus precipitation (bottom right, contour interval 2 mm day$^{-1}$, values greater than 4 mm day$^{-1}$ shaded), for the eastern North Pacific Ocean.

Fig. 9 shows the simulated incidence of LCI. Recall that LCI is assumed to occur when the air at the PBL top is supersaturated and the cloudtop entrainment stability criterion is not met. There is a tendency for LCI to occur downstream of regions where the PBL stratus incidence is high. This is particularly true for the eastern North Pacific. Prominent maxima of LCI incidence occur over the tropical and summer hemisphere continents; these maxima correspond very well with maxima in simulated cumulus activity. This is natural, since both cumulus convection and LCI are favored by high relative humidity at the PBL top and a weak inversion. It appears that, in regions of strongly diurnal cumulus activity, the GCM uses LCI to represent the effects of very shallow cumulus humilis clouds, which coexist with the deeper convective towers.

Fig. 10 shows a close-up view of the simulated July-mean PBL depth, PBL stratus depth, LCI incidence, and cumulus precipitation, for the marine stratocumulus regime of the eastern North Pacific Ocean. The simulated PBL depth increases from the California coast towards the southwest, in agreement with the observations of Neiburger et al. (1961). A region of frequent LCI separates the stratocumulus regime from the cumulus regime. The trade-winds associated with the California high carry PBL air from the stratus regime, through the LCI regime, and into the ITCZ. This model result is consistent with the discussion of LCI given by Randall (1980a).

Further detailed discussion of the baseline results is given by Randall et al. (1985).

## 4. SENSITIVITY EXPERIMENTS

### 4.1 Sensitivity of the GCM results to the parameterizations of stratocumulus entrainment and LCI.

In the design of the stratocumulus cloud parameterization, we have emphasized neither precipitation from the clouds nor the interaction of the clouds

with radiation. Instead, we have focused on the interaction between the clouds and the PBL turbulence. To study the impact of this key aspect of the stratocumulus parameterization on the results of the GCM, we have performed a two-month simulation, starting from June 1 of the second year of the three-year run and continuing to the end of July, in which the entrainment rate was determined without taking into account the effects of the clouds, and the parameterization of LCI was disabled. These two changes eliminated any direct interaction of the stratocumulus clouds with the PBL turbulence. However, we continued to check for the presence of PBL stratocumulus clouds in the usual way, and the clouds were recognized by the GCM's radiation parameterization in the usual way. Since, in this experiment, the entrainment parameterization did not take into account any sharp radiative cooling at cloud-top, we effectively assumed that the cooling was distributed uniformly through the depth of the mixed layer. For convenience, we refer to this as the "passive stratus" experiment.

We have compared the July-mean results of the experiment with the three-year composite July results presented earlier (hereafter, the "control"). Fig. 11 shows that the PBL stratocumulus clouds themselves are much more widespread in the experiment than in the control. The globally averaged stratus incidence is 32.7% in the experiment, versus 12.7% in the control, and the globally averaged stratus depths are 12.2 mb and 4.5 mb, respectively. The globally averaged relative humidity at the PBL top increases from 82.2% to 89.7%. The surface air temperature and the mixing ratio of the PBL both decrease, so the increased relative humidity is due to cooling rather than moistening. The increased stratocumulus cloudiness of the experiment occurs over both land and ocean, but is particularly noticeable over the subtropical oceans. The globally averaged total cloudiness is significantly increased, from 49.1% to 59.9%. Surprisingly, the changes

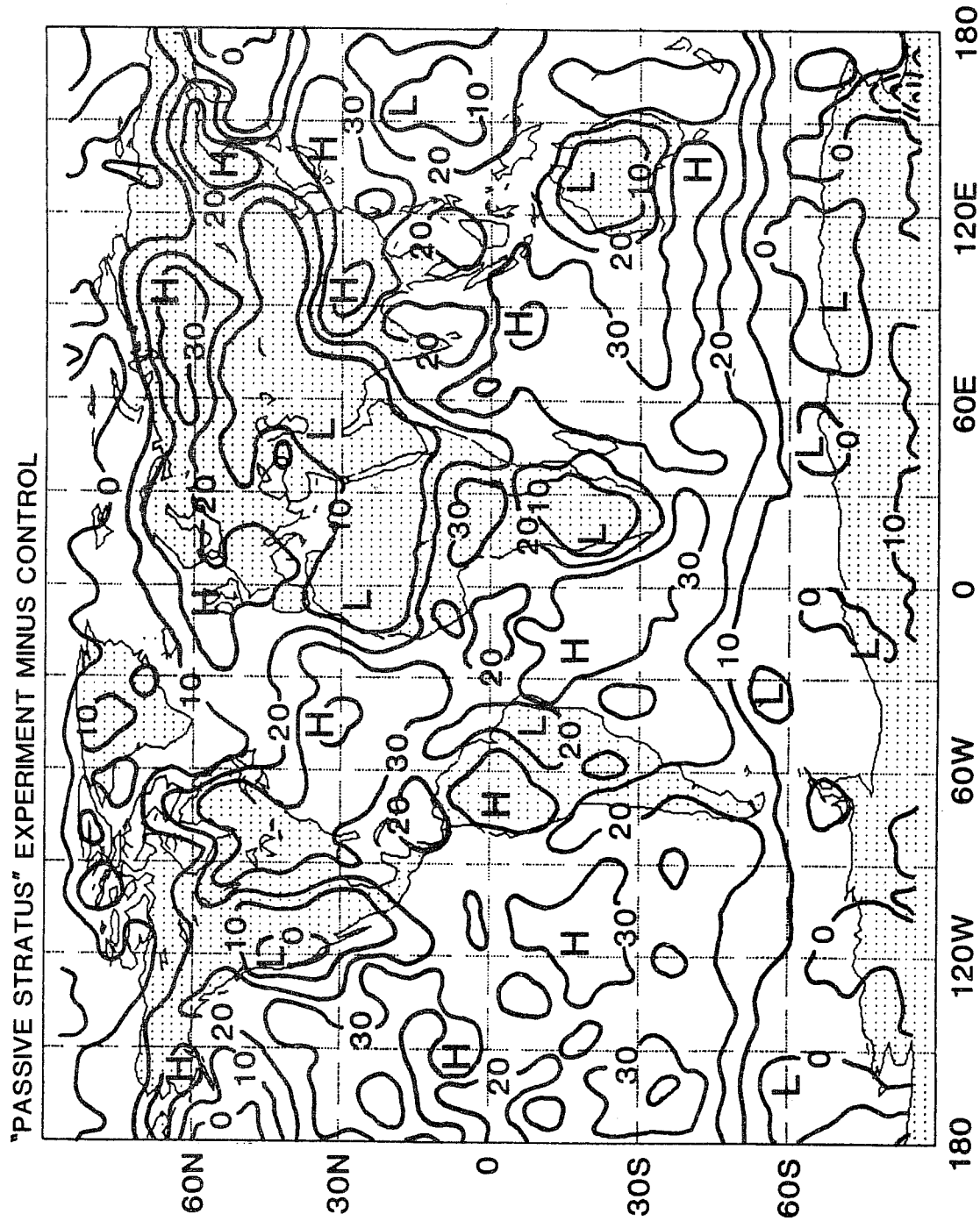


Figure 11. Diference in simulated stratus incidence between the "passive stratus" experiment and the control. The contour interval is 10%.

in the PBL depth distribution are not very dramatic; the PBL deepens slightly over the oceans.

The planetary radiation budget is noticeably perturbed in the experiment. The net solar flux at the top of the atmosphere decreases by 24.1 W $m^{-2}$, from 236.6 W $m^{-2}$, to 213.3 W $m^{-2}$, and the planetary albedo increases dramatically from 28.0% to 35.1%. However, the outgoing terrestrial radiation decreases only slightly, from 237.0 W $m^{-2}$ to 233.2 W $m^{-2}$. As a result, the July-mean planetary radiation budget is shifted by 18.7 W $m^{-2}$, from near-balance in the control to cooling in the experiment.

The sensible heat budgets of the PBL and the earth's surface are also noticeably modified in the experiment. The longwave radiative cooling of the PBL dramatically increases, from 3.95 K $day^{-1}$ to 8.41 K $day^{-1}$, as a result of the increased PBL cloudiness. Although the globally averaged surface latent heat flux hardly changes at all, the surface sensible heat flux increases from 1.9 W $m^{-2}$ to 10.1 W $m^{-2}$, tending to counteract the increased radiative cooling of the PBL. The surface buoyancy flux also increases sharply. The net upward terrestrial radiation at the earth's surface decreases from 79.7 W $m^{-2}$ to 64.8 W $m^{-2}$. This is mostly due to an increase in the downward component of the net flux, from 323.0 W $m^{-2}$ to 336.6 W $m^{-2}$. The net downward surface solar radiation has decreased from 197.4 W $m^{-2}$ to 173.3 W $m^{-2}$. The total surface heat flux has changed in the direction of cooling the ocean, from -3.2 W $m^{-2}$ to -22.0 W $m^{-2}$. Most of the change in the total surface heat flux occurs over the tropical and Northern Hemisphere (summer) oceans.

The results of this experiment show that the interaction between stratocumulus clouds and the PBL turbulence strongly influences the global distributions of both low and total cloudiness. The absence of LCI in the experiment seems to be primarily responsible for the increased cloudiness.

However, the stratus incidence in the experiment is considerably larger than the sum of the stratus incidence and LCI incidence in the control. In the experiment, clouds that would otherwise have been destroyed by LCI cause a cooling of the PBL through long-wave radiation. This tends to increase the relative humidity of the PBL, and so leads to more extensive low-level cloudiness, which, in turn, causes a large deficit in the earth-atmosphere radiation budget. Unrealistically extensive low clouds are a common problem in many GCMs with predicted clouds (e.g. Wetherald and Manabe, 1980; Shukla et al., 1982; Slingo, 1982). The results of our "passive stratus" experiment indicate that this problem is at least partially due to a failure to take into account the interaction of the low clouds with PBL turbulence.

4.2 Sensitivity of the GCM results to the variability of the PBL depth.

We have chosen to make the PBL depth a prognostic variable of the GCM in order to take into account the effects of PBL-depth variability in determining the effects of the surface fluxes (Deardorff, 1972) and in controlling the interaction of the PBL with cumulus convection (Arakawa and Schubert, 1974). To study the sensitivity of the model results to the variability of the PBL depth, we have performed a two-month simulation, starting from June 1 of the second year of the control and continuing to the end of July, in which the PBL depth was fixed everywhere and throughout the run at 43.95 mb. This globally uniform value is the same as the globally averaged PBL depth for July of the second year of the control, and is very close to the three-year composite July mean PBL depth. It is higher than the average for land points in the control, and lower than the average for ocean points. For convenience, we refer to this as the "fixed PBL" experiment. A physical interpretation of the fixed-PBL-depth constraint is that the entrainment rate takes whatever value is needed to balance the PBL mass

sources and sinks due to large-scale convergence and/or cumulus convection.

We have compared the July-mean results of the experiment with the three-year composite July results presented earlier. As already mentioned, the PBL is deeper over land in the experiment, and shallower over the oceans. This leads to a straightforward global redistribution of PBL stratus cloudiness: The stratus incidence increases over land and decreases over the oceans, simply because a high PBL top is more likely to be above the condensation level. The stratus incidence decreases in the Southern Hemisphere, and increases in the high latitudes of the Northern Hemisphere. Although the globally averaged stratus incidence hardly changes, LCI incidence increases dramatically, practically everywhere. This suggests that if it were not for LCI, the global stratus incidence would have increased in the experiment. The simulated total cloudiness increases over eastern North America, South America, equatorial Africa, India, the southwestern Pacific, and the Arctic Ocean. It decreases over the South Atlantic and Indian Oceans. Cumulus activity is much greater globally in the experiment, particularly over land and over the winter-hemisphere oceans. The globally averaged cumulus mass flux increases from 0.65 mb $hr^{-1}$ to 0.96 mb $hr^{-1}$. Although the globally averaged total precipitation decreases slightly, the convective precipitation increases dramatically, especially over land. Fig. 12 shows the July-mean simulated convective precipitation for the experiment. The rainfall rate has increased unrealistically over northern Africa, India, and eastern North America, but the precipitation of the ITCZ has weakened over both the Atlantic and the eastern Pacific. The evaporation rate decreases over both land and ocean; and the excess of precipitation over evaporation increases markedly over land, from -0.04 mm $dy^{-1}$ to 0.91 mm $dy^{-1}$, so that the continents become strong moisture sinks for the July atmosphere. Observations (Rasmusson 1967, 1968; Baumegartner and Reichel, 1975) suggest that in this respect the results of the control are much

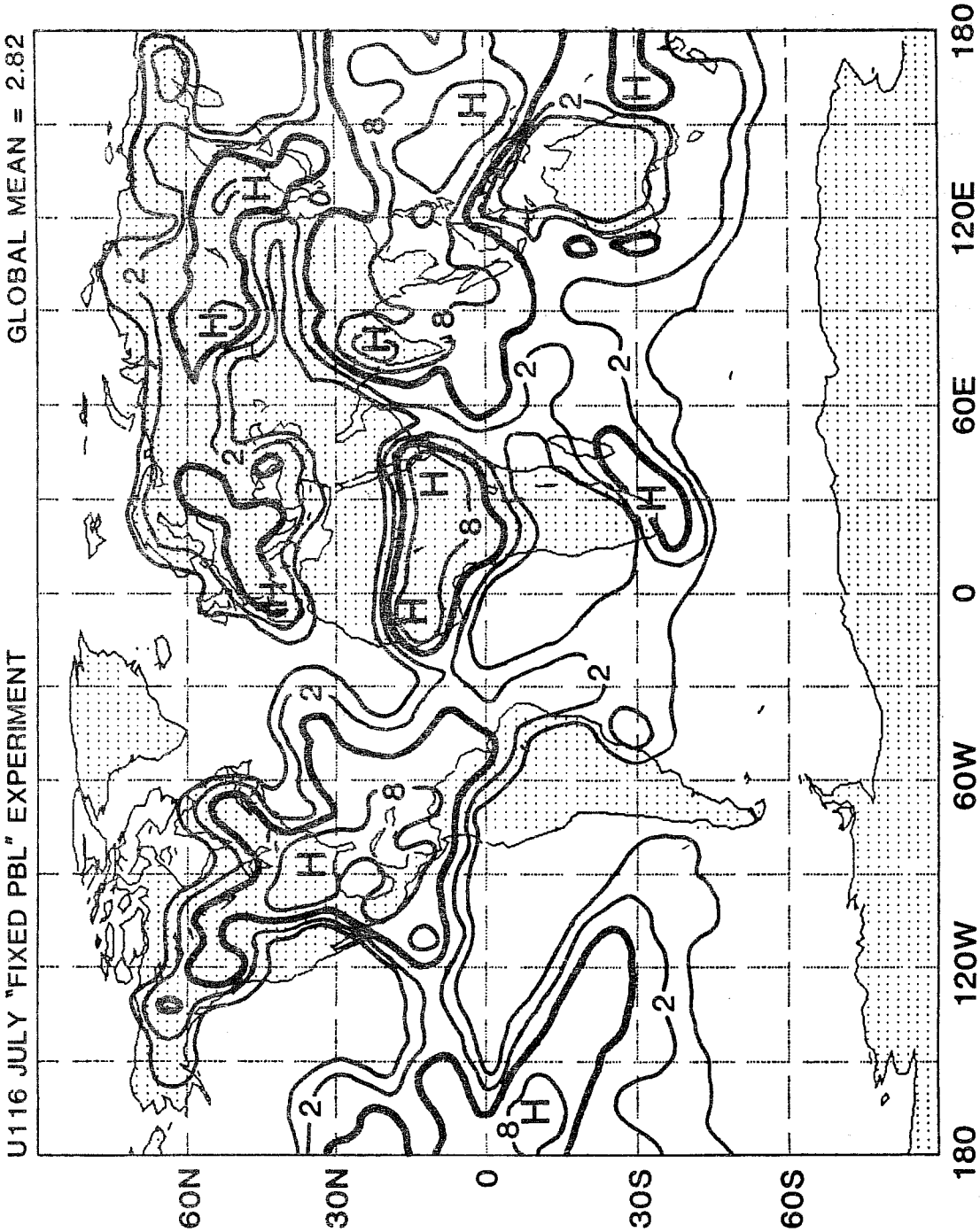


Figure 12. Simulated cumulus precipitation for the "fixed PBL" experiment. The contours plotted are 1, 2, 4 (heavy), 8, and 16 mm day$^{-1}$.

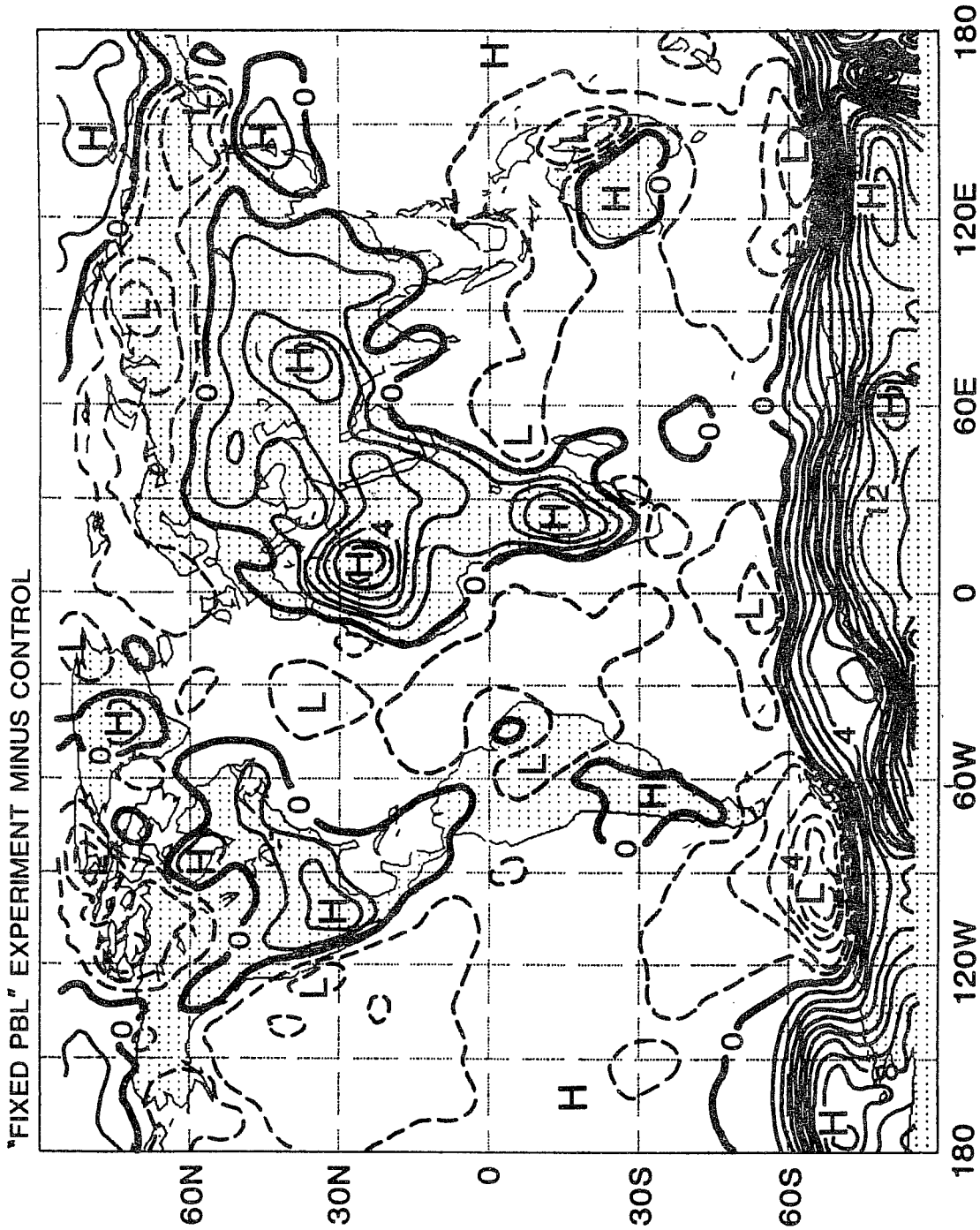


Figure 13. Difference in simulated surface air temperature between the "fixed-PBL" experiment and the control. The contour interval is 1°C.

more realistic than those of the experiment.

The increased cumulus precipitation in the experiment can be understood in terms of the interaction of the PBL with cumulus convection. Although a deep PBL is favorable for cumulus activity, the cumulus clouds tend to make the PBL shallow by drawing on its mass (Arakawa and Schubert, 1974) . By fixing the PBL depth in the experiment, we have cut this negative feedback loop that normally helps to control the intensity of cumulus activity. The increase in the convective precipitation rate is particularly large over land, because the time-averaged continental PBL depth is considerably increased in the experiment. However, the diurnal variation of cumulus convection over land in the experiment is qualitatively similar to that of the control. The maximum is greater in amplitude, but occurs at about the same local time.

The surface turbulent fluxes and the PBL bulk properties are also significantly modified in the experiment. The PBL wind speed increases globally, and particularly over land. The PBL mixing ratio increases over the ocean, but it decreases over land, even though, as noted earlier, the evaporation rate decreases over both land and ocean. As shown in Fig. 13, the surface air temperature rises over land, particularly in desert regions, but it decreases over the oceans and globally. The surface sensible heat flux increases strongly over both land and ocean. These results show that the surface energy balance established by the model is sensitive to the variability of the PBL depth.

The sea-level pressure is reduced, in the experiment, over North America, Africa, Europe, and the Tibetan Plateau. These relative lows are associated with the increased precipitation in the same regions. The sea-level pressure is increased on the poleward and westward sides of the subtropical highs.

The results of this experiment show that the variability of the PBL depth influences the general circulation primarily by regulating the intensity of cumulus convection over land. There are also significant effects on the surface energy balance and the distribution of low stratiform clouds.

4.3 Sensitivity of the GCM results to the diurnal cycle of solar radiation. Even today, many comprehensive GCMs use a daily mean insolation in place of the true diurnally varying insolation. The earliest version of the UCLA GCM also used a daily mean insolation (Mintz, 1965), but since about 1970 all versions of the UCLA model have included the diurnal cycle, and in fact the diurnal forcing of the planetary boundary layer and cumulus convection over the continents has significantly influenced our thinking in recent years (Randall, 1976; Suarez et al., 1983). Some examples of the diurnal variability simulated by recent versions of the UCLA GCM are given by Randall (1976), Suarez et al. (1983), and Randall et al. (1985). We have performed a two-month simulation, starting from June 1 of the second year of the control and continuing to the end of July, in which the diurnal cycle was artificially suppressed. On each time-step, and for each longitude, the cosine of the solar zenith angle was assigned its (true) zonally averaged value for that latitude. (Of course, negative values were replaced by zeros before taking the zonal mean.) We refer to this as the "torroidal sun" experiment.

The July-mean continental PBL depth increases from 29.56 mb in the control to 54.74 mb in the experiment. Not surprisingly, in the absence of a diurnal cycle the average PBL depth over land is comparable to that over the oceans.

There are very interesting changes in the planetary radiation budget. Although the globally averaged total cloudiness decreases slightly (primarily over the oceans), the planetary albedo actually increases by three percent!

The reason is that in the control run there is a tendency for more cloudiness to occur on the night side of the earth. According to J. Susskind of GLAS (personal communication, 1984), multichannel satellite retrievals based soley on terrestrial radiation consistently show greater global cloudiness at night than at day, so this model result appears to be realistic. The net outgoing longwave flux at the top of the atmosphere increases slightly in the experiment, consistent with the small reduction in total cloudiness. The total radiation at the top of the atmosphere shifts in the direction of cooling the earth, by about 14 W $m^{-2}$.

The surface energy budget is also significantly altered. Although the net surface solar flux decreases by about 15 W $m^{-2}$ (consistent with the increased planetary albedo), the globally averaged net longwave flux at the surface is unchanged, and over land the net longwave flux actually increases by 6 W $m^{-2}$. The turbulent sensible and latent heat fluxes decrease over land, to maintain the land-surface energy balance. The oceans experience a strong net cooling in the experiment; the net outward flux of energy from the oceans is 25 W $m^{-2}$.

The globally averaged total precipitation is almost unchanged in the experiment, but over land it increases sharply, from 3.76 mm $day^{-1}$ to 5.51 mm $day^{-1}$, while over the oceans it decreases from 4.21 mm $day^{-1}$ to 3.55 mm $day^{-1}$. Essentially all of the change is in the convective part of the precipitation. These results are similar to those found in the "fixed PBL" experiment, but more pronounced. As shown in Fig. 14, the geographical distribution of the difference between precipitation and evaporation shifts radically in the experiment, so that the July continents experience a net excess of precipitation, in the amount of 2.11 mm $day^{-1}$. The Atlantic ITCZ rainbelt is completely missing, while the Sahel receives plentiful rainfall. Suprisingly, the evaporation over land actually decreases

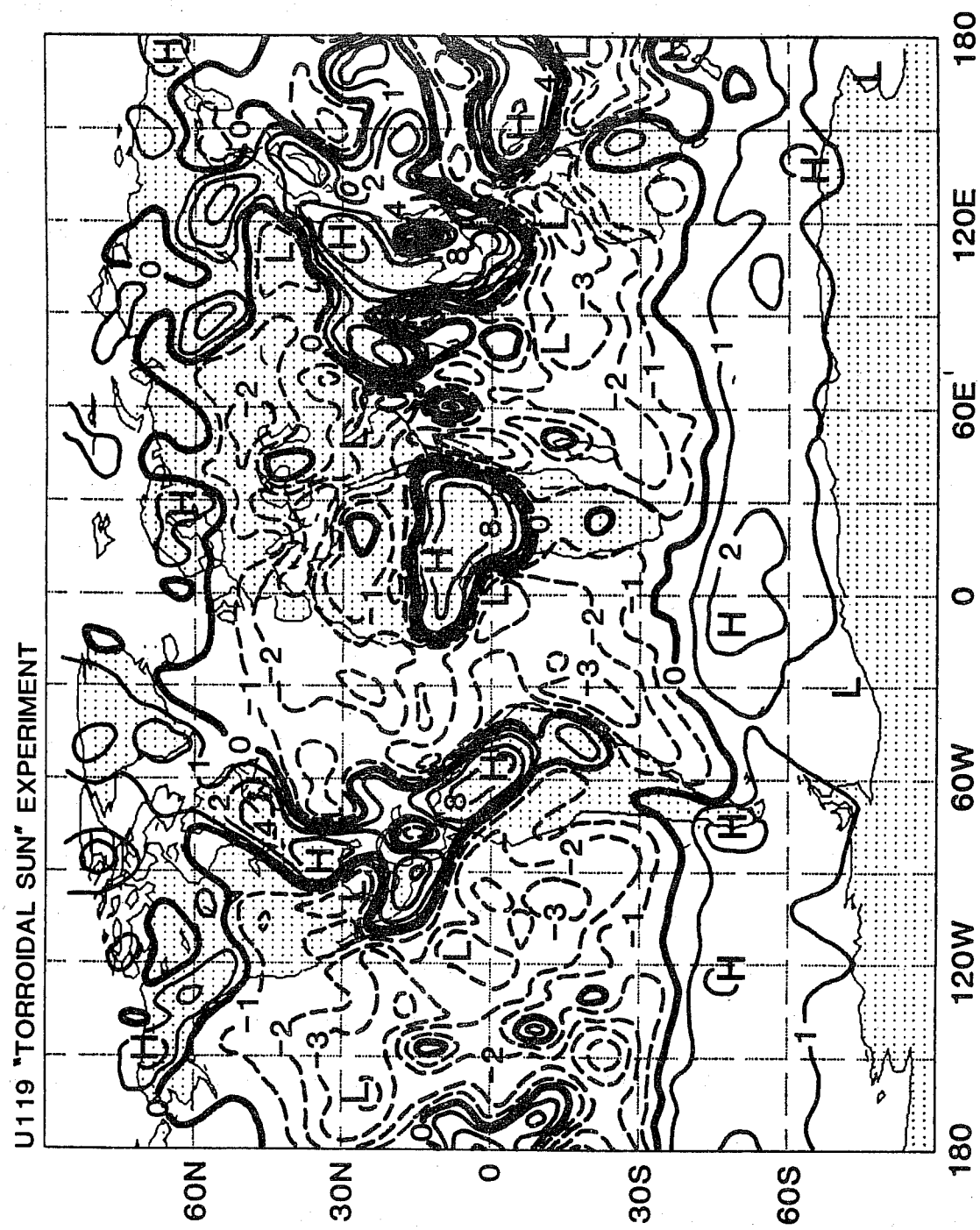


Figure 14. Simulated difference between preciptation and evaporation for the "torroidal sun" experiment. The contours plotted are -4, -3, -2, -1, 0 (heavy), 1, 2, 4, 8, and 16 mm day$^{-1}$.

in the experiment, while that over the oceans increases! This shows that the additional precipitation over land is supplied by increased convergence of moisture from the oceans. Apparently a "continental-scale sea breeze" is set up (or enhanced) in the torroidal sun experiment. In the control run, the diurnal cycle interferes with the development of such a circulation. Observations (Rasmusson, 1967, 1968; Baumegartner and Reichel, 1975) show that the atmospheric water balance of our "torridal sun" experiment is much less realistic than that of the control.

Fig. 15 shows the simulated velocity potential for the 200 mb surface. The region of 200 mb convergence over northern Africa, which is present throughout the year in both the control run and the observations, has practically disappeared in the experiment. This is consistent with the increased African rainfall discussed above. The center of 200 mb convergence over southern Africa has shifted westward, to the South Atlantic Ocean.

The results of our "torroidal sun" experiment show that the land-sea contrast in the strength of the diurnal cycle exerts a powerful influence on the partitioning of July precipitation between the continents and the oceans, by tending to reduce the precipitation rate over land. The diurnal cycle also has a strong effect on the energy budgets at the earth's surface and the top of the atmosphere, and it significantly modifies the time-averaged distribution of PBL depth. Evidently the diurnal cycle cannot be neglected as a detail, even for climate simulations.

## 5. SIMULATIONS WITH A REVISED RADIATION PARAMETERIZATION.

We have recently adopted new parameterizations of solar and terrestrial radiation. The former is based on the work of Lacis and Hansen (1974), as modified by Davies (1982) and further revised by Harshvardhan and Corsetti (1984) and Harshvardhan et al. (1985). In addition to including the zenith-angle dependence of cloud and surface albedoes, the new solar radiation

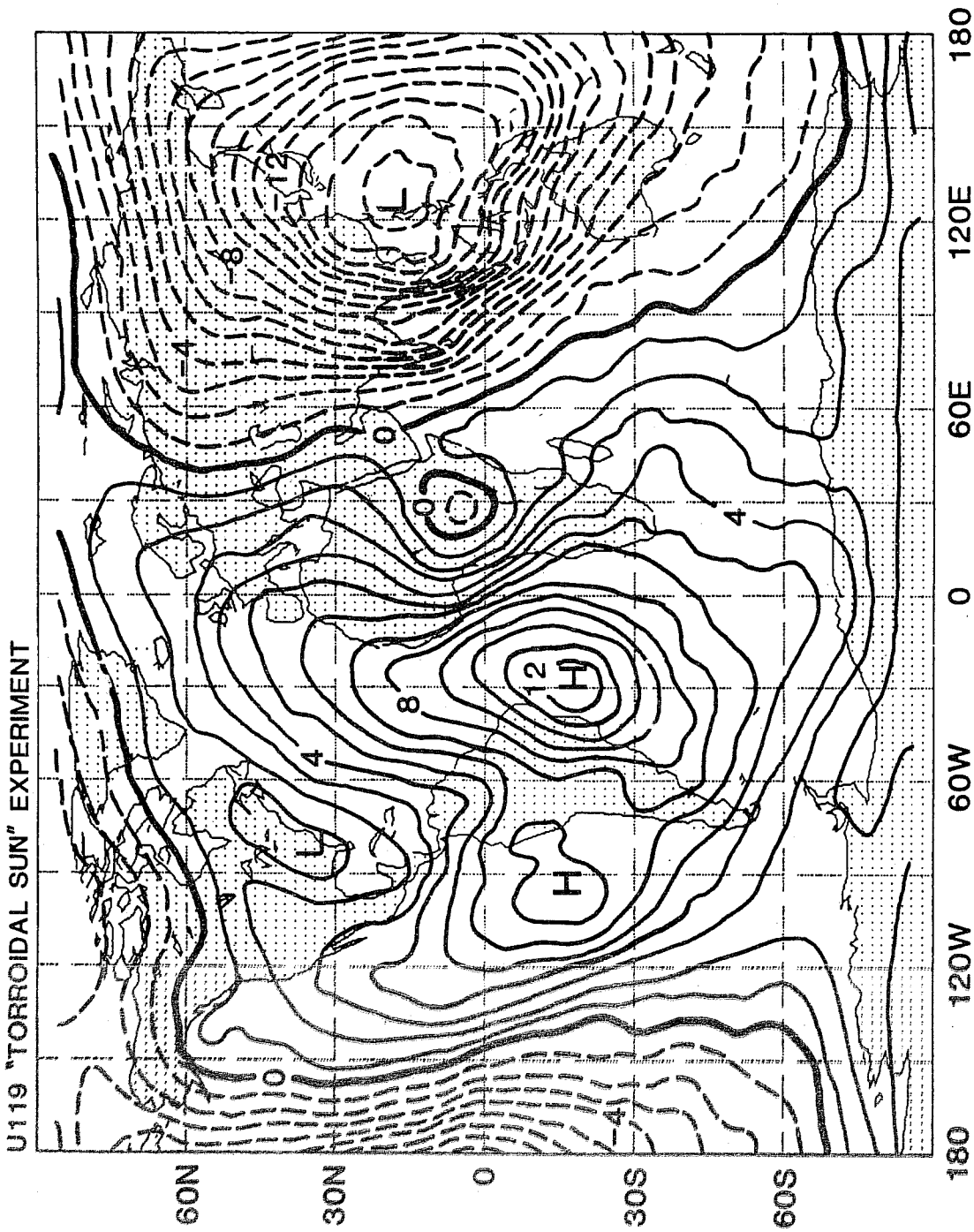


Figure 15. Simulated 200 mb velocity potential for the "torroidal sun" experiment. The contour interval is $10^6$ $m^2$ $s^{-1}$, the zero contour is heavy, and negative contours are dashed.

parameterization allows a flexible prescription of cloud optical depths. The new terrestrial radiation parameterization includes water vapor effects as proposed by Chou (1984), carbon dioxide emission as suggested by Chou and Peng (1983), and ozone emission as discussed by Rodgers (1968). A description is given by Harshvardhan and Corsetti (1984). An important change is that the new parameterization includes the effects of "continuum" or "e-type" water vapor emission (Cox and Griffith, 1979). This leads to increased PBL cooling, particularly in the humid tropics (Tables 1 and 2).

In the solar radiation calculation, the optical thickness of the clouds is assumed to be proportional to the pressure thickness, and also to increase with temperature. In the terrestrial radiation, cirrus (sufficiently cold) clouds are assumed to have emissivities of 0.5, and sufficiently thin PBL stratus clouds are assumed to have emissivities which decrease to zero as the cloud becomes arbitrarily thin. We have also corrected a coding error which caused cumulus anvils to be ignored in the radiation calculation.

Preliminary results obtained with the revised radiation parameterizations are presented in this Section. The new parameterizations have led to substantial improvements in the simulation of the PBL. The e-type cooling of the PBL has had several direct and favorable consequences. First, the radiative cooling of the PBL has increased substantially over the oceans, particularly in the tropics (Fig. 16). Over land, the cooling has actually decreased, for the following reason. The shallow nocturnal PBL is overlain by moist air which has been transported up to higher levels during the previous afternoon. The moist upper layer is fairly opaque to infrared radiation, largely because of continuum absorption, and so it acts as a thermal blanket to reduce the cooling of the nocturnal PBL. Because the time-averaged radiative cooling of the PBL has increased over the oceans and decreased over the land, the land-sea contrast in cooling evident in

Table 1: Radiative cooling rates obtained for the tropical sounding of McClatchey et al. (1972), with and without "e-type" cooling.

| PRESSURE (mb) | | COOLING RATES, K DAY$^{-1}$ | |
|---|---|---|---|
| FROM | TO | WITH E-TYPE | W/O E-TYPE |
| 1.0 | 1.9 | 7.22 | 7.21 |
| 1.9 | 3.7 | 6.53 | 6.50 |
| 3.7 | 7.2 | 4.51 | 4.47 |
| 7.2 | 13.9 | 2.92 | 2.87 |
| 13.9 | 26.8 | 1.40 | 1.33 |
| 26.8 | 51.8 | 0.06 | -0.01 |
| 51.8 | 100.0 | -0.06 | -0.09 |
| 100.0 | 152.6 | 0.03 | 0.02 |
| 152.6 | 223.4 | 0.38 | 0.37 |
| 223.4 | 314.9 | 1.72 | 1.71 |
| 314.9 | 431.4 | 2.42 | 2.40 |
| 431.4 | 575.5 | 2.13 | 2.03 |
| 575.5 | 751.6 | 1.95 | 1.61 |
| 751.6 | 963.0 | 2.72 | 1.39 |
| 963.0 | 1013.0 | 3.06 | 1.24 |

Table 2: Radiative fluxes obtained for the tropical sounding of McClatchey et al. (1972), with and without "e-type" cooling.

| FLUX (W m $^{-2}$) | WITH E-TYPE | W/O E-TYPE |
|---|---|---|
| $F\uparrow$ top of atmosphere | 297.1 | 307.1 |
| $F\downarrow$ surface | 390.4 | 326.5 |
| $F^{\uparrow}_{net}$ surface | 68.9 | 132.8 |

the baseline run (Fig. 7) is greatly reduced with the new radiation parameterization.

The increased radiative cooling of the oceanic PBL is balanced by an increase in the surface sensible heat flux, toward more realistic values (Fig. 17). It also leads to a welcome increase in the relative humidity at the PBL top, particularly in the tropics (Fig. 18). Finally, it increases the incidence of PBL stratocumulus clouds (Fig. 19), particularly in coastal regions and in high latitudes. These changes represent an improvement in the simulated boundary-layer climate.

As discussed by Randall et al. (1985), in the baseline runs the model did not produce any systematic diurnal variation of precipitation over the sea, even though the diurnal variation over land was very pronounced. This has changed now that the radiative effects of cumulus anvils are included in the model. Currently, any cumulus towers penetrating above the 500 mb level are assumed to produce complete overcast from that level to the cloud tops. Fig. 20 shows the simulated diurnal variation of precipitation, composited for the 24 ocean grid points shown in Fig. 1 of Randall et al. (1985). Nocturnal precipitation dominates, with a maximum near sunrise; daytime precipitation is suppressed. For these 24 grid points, the amplitude of the oceanic diurnal precipitation cycle is about 1.2 mm $day^{-1}$, compared with a mean of 3.7 mm $day^{-1}$. Much stronger diurnal precipitation cycles are found at individual oceanic grid points, particularly in the tropics. These model results are in qualitative agreement with observations reported by Gray and Jacobsen (1977). The mechanisms through which diurnal solar forcing induces a diurnal maritime precipitation cycle are currently being investigated. The roles of both direct radiative effects and radiatively induced vertical motions are being assessed.

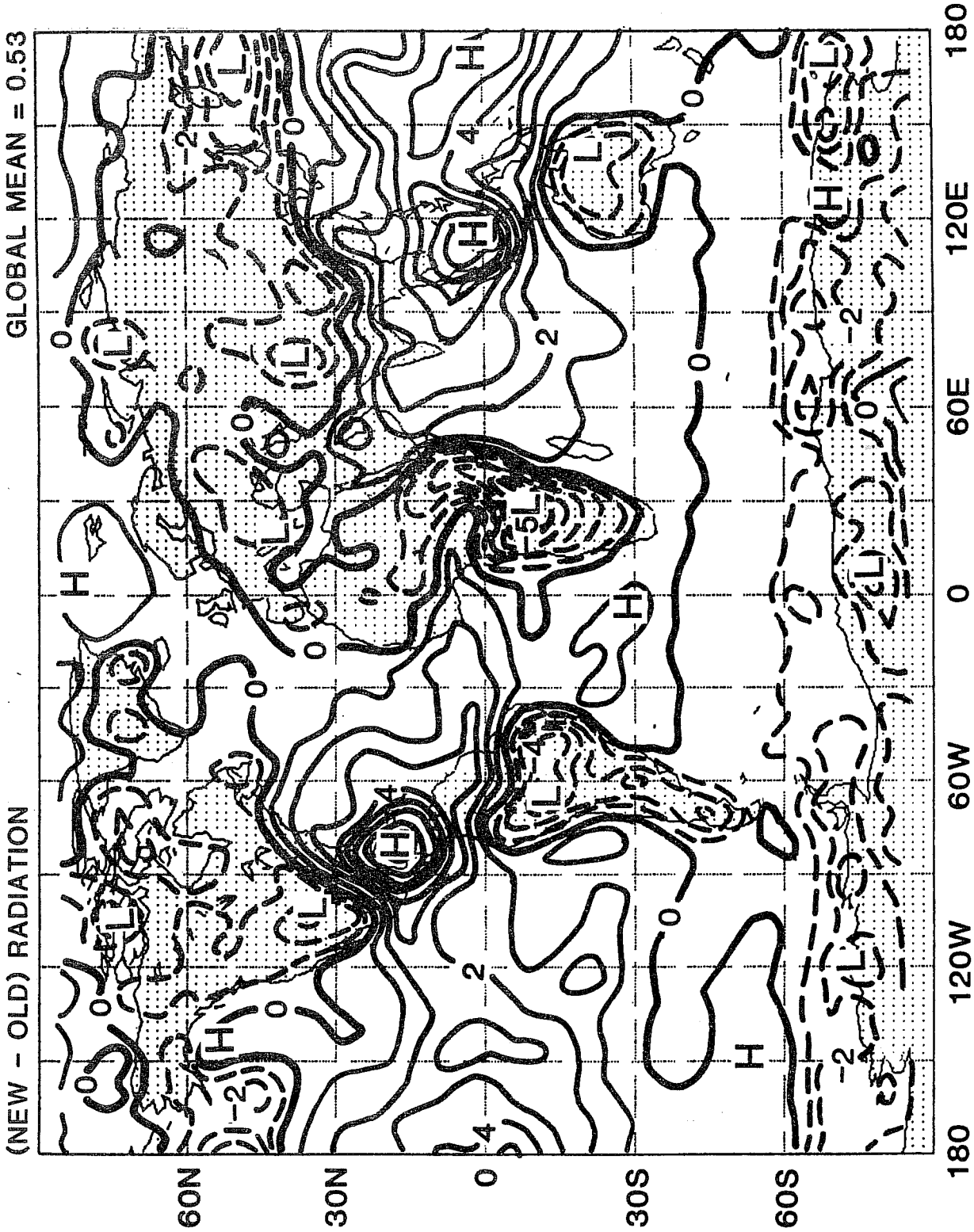


Figure 16. Change in July longwave radiative cooling of the PBL resulting from the use of the new radiation parameterization. The contour interval is 1 W $m^{-2}$, the zero contour is heavy, and negative contours are dashed.

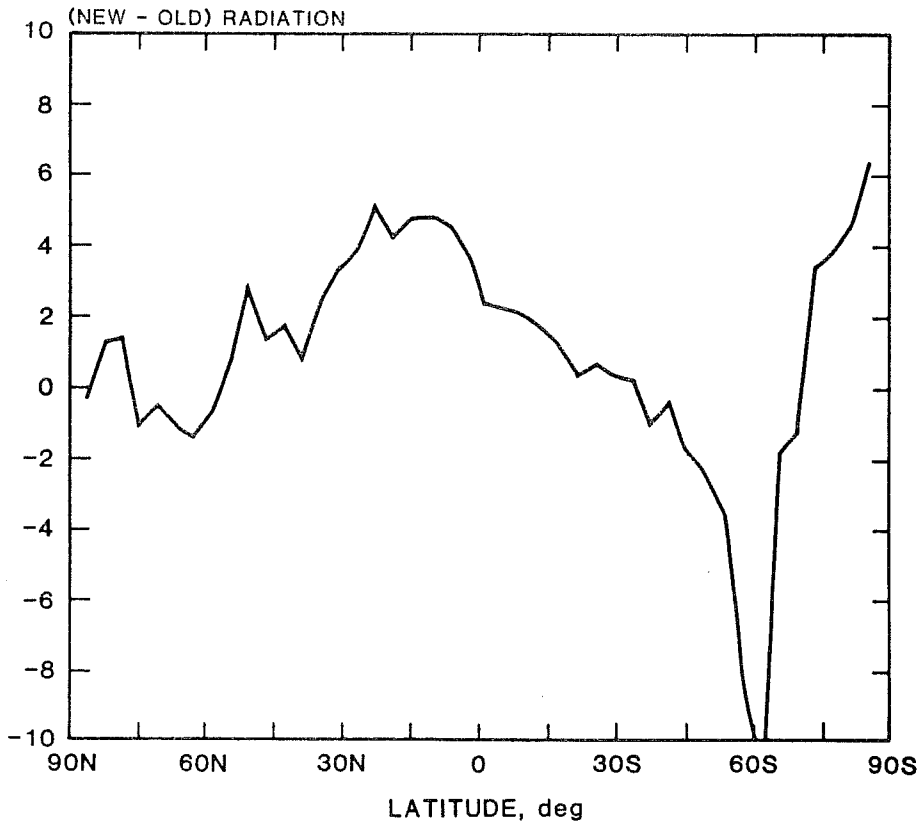


Figure 17. Zonally averaged change in the surface sensible heat flux resulting from the use of the new radiation parameterization.

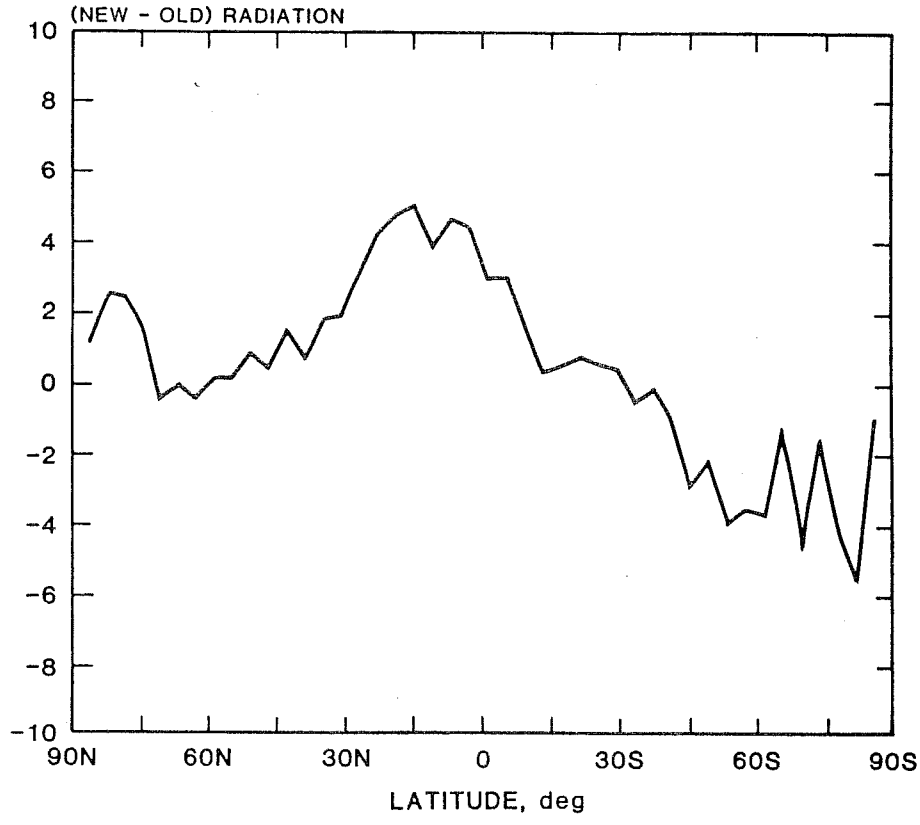


Figure 18. Zonally averaged change in the relative humidity at the PBL top resulting from the use of the new radiation parameterization.

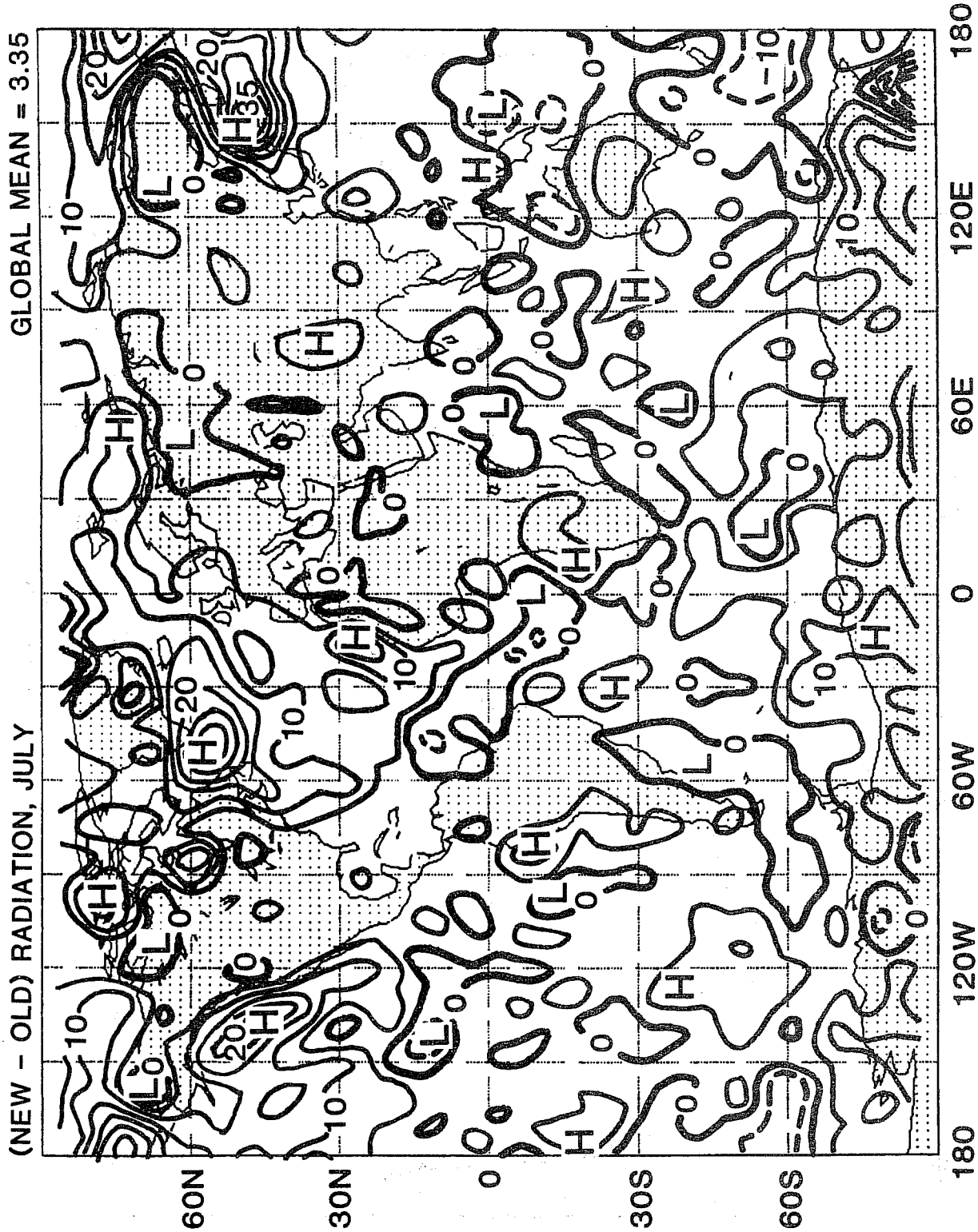


Figure 19. Change in the PBL stratus incidence resulting from the use of the new radiation parameterization. The contour interval is 5%, the zero contour is heavy, and negative contours are dashed.

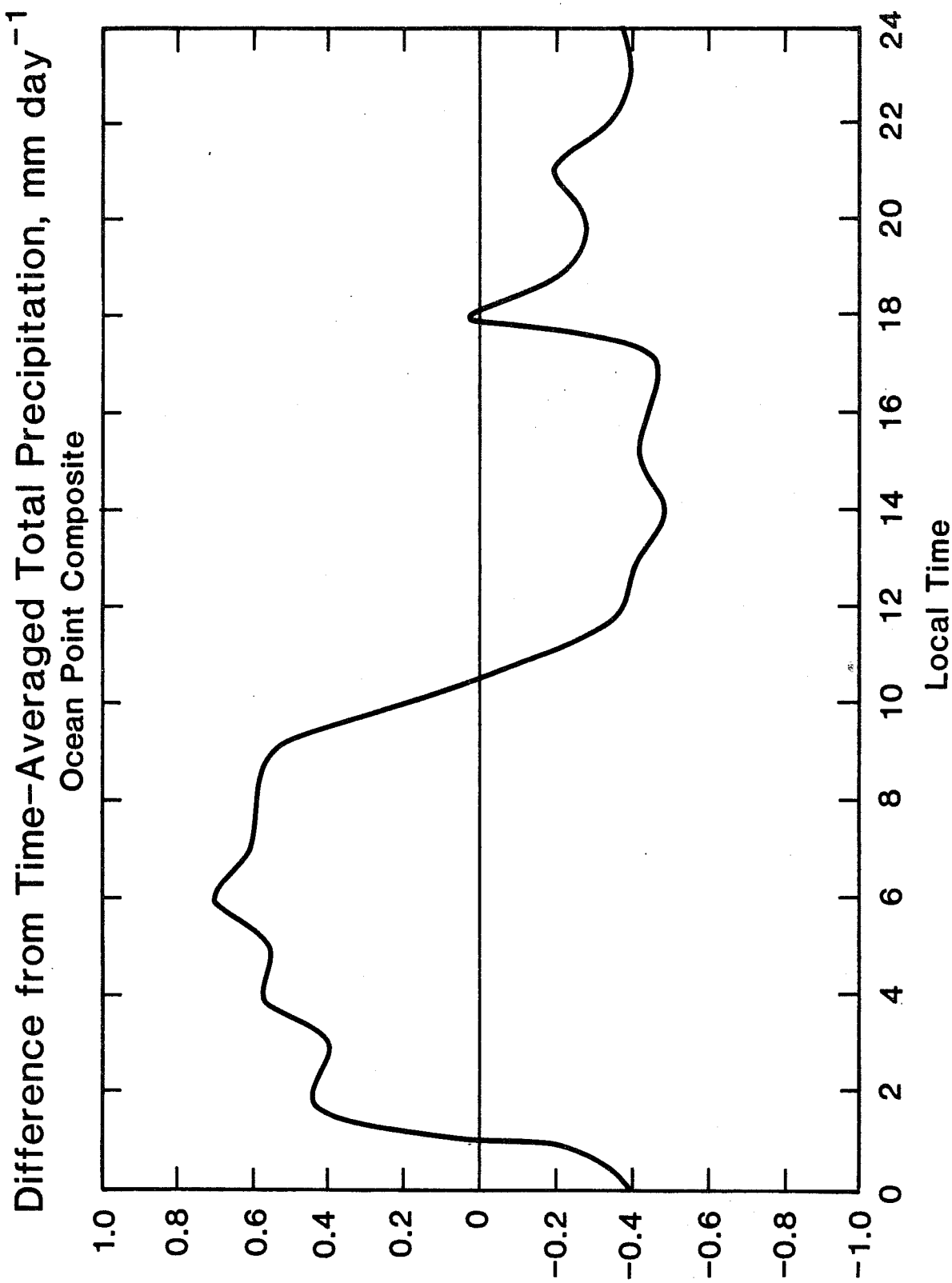


Figure 20. Simulated departure of the total precipitation rate from the time mean, as a function local time of day, composited for 24 ocean grid points.

## 6. CONCLUDING REMARKS

In the near future, we plan to test the sensitivity of the model results to the vertical resolution, and to the assumptions used to determine the properties of the air just above the PBL top. We also plan to include the effects of distributed radiative cooling and warming on the entrainment rate of a cloud-topped mixed layer.

## ACKNOWLEDGEMENTS

Prof. Akio Arakawa of UCLA is the chief architect of the UCLA general circulation model.

Dr. Harshvardhan of the University of Maryland developed the new radiation parameterization discussed in this paper. Tom Corsetti provided first-rate programming assistance. Mary Ann Wells typed the manuscript, and Laura Rumburg prepared the figures.

This research has been sponsored by NASA's Climate Program Office. I am grateful to ECMWF for making my participation in this Workshop possible.

## REFERENCES

Arakawa, A., and W. H. Schubert, 1974: The interaction of a cumulus cloud ensemble with the large-scale environment, Part I. J. Atmos. Sci., 31, 674-701.

Arakawa, A., and V. R. Lamb, 1977: Computational design of the basic dynamical processes of the UCLA general circulation model. Methods in Computational Physics, 17, Academic Press, New York, 173-265.

Arakawa, A., and V. R. Lamb, 1981: A potential enstrophy and energy conserving scheme for the shallow water equations. Mon. Wea. Rev., 109, 18-36.

Arakawa, A., and M. J. Suarez, 1983: Vertical differencing of the primitive equations in sigma coordinates. Mon. Wea. Rev., 111, 34-45.

Baumegartner, A., and E. Reichel, 1975: The World Water Balance. Elsevier Scientific Publ. Co., Amsterdam, 179 pp.

Berliand, T. G., and L. A. Strokina, 1980: Global distribution of the total amount of cloudiness. Hydrometeorology Publishing House, Leningrad, 71 pp. (in Russian).

Brooks, C. E. P., 1927: The mean cloudiness over the earth. Memoirs of the Royal Meteorological Society, 1, 127-138.

Chou, M.-D., 1984: Broadband water vapor transmission functions for atmospheric IR flux computations. J. Atmos. Sci., 41, 1775-1778.

Chou, M.-D., and L. Peng, 1983: A parameterization of the absorption in the 15 μm $CO_2$ spectral region with application to climate sensitivity studies. J. Atmos. Sci., 40, 2183-2192.

Chou, S.-H., and D. Atlas, 1982: Satellite estimates of ocean-air heat fluxes during cold air outbreaks. Mon. Wea. Rev., 110, 1434-1450.

Crane, R. G., and R. G. Barry, 1984: The influence of clouds on climate with a focus on high-latitude interactions. J. Climatology, 4, 71-93.

Cox, S. K., and K. T. Griffith, 1979: Eximates of radiative divergence during Phase III of the GARP Atlantic Tropical Experiment: Part II. Analysis of Phase III results. J. Atmos. Sci., 36, 586-601.

Davies, R., 1982: Documentation of the solar radiation code in the GLAS GCM. NASA Tech. Memo. 83961, 57 pp.

Deardorff, J. W., 1972: Parameterization of the planetary boundary layer for use in general circulation models. Mon. Wea. Rev., 100, 93-106.

Esbensen, S. K., and Y. Kushnir, 1981: The heat budget of the global ocean: An atlas based on estimates from surface marine observations. Climatic Research Institute Report No. 29, Oregon State University, Corvallis, OR 97331.

Gray, W. M., and R. W. Jacobsen, Jr., 1977: Diurnal variation of oceanic deep cumulus convection. Mon. Wea. Rev., 105, 1171-1188.

Hahn, C. J., S. G. Warren, J. London, R. M. Chevin, and R. Jenne, 1982: Atlas of simultaneous occurrence of different cloud types over the ocean. NCAR Tech. Note TN-201, 212 pp.

Harshvardhan, and T. G. Corsetti, 1984: Longwave radiation parameterization for the UCLA/GLAS GCM. NASA Tech. Memo. 86072, 51 pp.

Harshvardhan, R. Davies, D.A. Randall, and T. G. Corsetti, 1985: An efficient radiation parameterization for use in general circulation models. Manuscript in preparation.

Herman, G., and R. Goody, 1976: Formation and persistence of summertime Arctic stratus clouds. J. Atmos Sci., 33, 1537-1553.

Huschke, R. E., 1969: Arctic cloud statistics from air-calibrated surface weather observations. RAND Memorandum RM-6173-PR, 79 pp.

Kraus, E. B., 1963: The diurnal precipitation change over the sea. J. Atmos. Sci., 20, 551-556.

Lacis, A. A., and J. E. Hansen, 1974: A parameterization for the absorbtion of solar radiation in the earth's atmosphere. J. Atmos. Sci., 31, 118-133.

London, J., 1957: A study of the atmospheric heat balance. Final Report, Contact No. AF19(122)-165, Dept. of Meteorology and Oceanography, New York University, New York, 99 pp.

Lord, S. J., W. C. Chao, and A. Arakawa, 1982: Interaction of a cumulus cloud ensemble with the large-scale environment. Part IV. The discrete model. J. Atmos. Sci., 39, 104-113.

McClatchey, R. A., R. W. Fenn, J. E. A. Selby, F. E. Volz, and J. S. Garing, 1972: Optical properties of the atmosphere (Third edition). AFCRL-047297, 108 pp (NTIS # AD753075).

Miller, D. B., and R. G. Feddes, 1971: Global atlas of relative cloud cover 1967-1970. Joint production by U.S. Dept. of Commerce and U.S. Air Force. Washington, DC, September, 1971.

Mintz, Y., 1965: Very long-term global integration of the primitive equations of atmospheric motion: (an experiment in climate simulation). Amer. Met. Soc. Meteorological Monographs, 8, pp 20-36.

Neiburger, M., Johnson, D. S and Chien, C.-W., 1961: Studies of structure of the atmosphere over the eastern Pacific ocean in summer. I. The inversion over the eastern north Pacific Ocean. University of California Press. Berkeley and Los Angeles.

Ninomiya, K., and T. Akiyama, 1976: Structure and heat energy budget of mixed layer capped by inversion during the period of polar outbreak over Kuroshio region. J. Met. Soc. Japan, 54, 117-131.

Randall, D. A., 1976: The interaction of the planetary boundary layer with largescale circulations. Ph.D. Thesis, The University of California, Los Angeles, 247 pp.

Randall, D. A., 1979: The entraining moist boundary layer. Preprint volume, Fourth Symposium on Turbulence, Diffusion, and Air Pollution of the Amer. Meteor. Soc., Reno, Nevada, 467-470. (Available from the author at the Goddard Laboratory for Atmospheric Sciences, NASA/Goddard Space Flight Center, Code 611, Greenbelt, MD 20771.

Randall, D. A., 1980a: Conditional instability of the first kind, upside-down. J. Atmos. Sci., 37, 125-130.

Randall, D. A., 1980b: Entrainment into a stratocumulus layer with distributed radiative cooling. J. Atmos. Sci., 37, 148-159.

Randall, D. A., 1984a: Buoyant production and consumption of turbulence kinetic energy in cloud-topped mixed layers. J. Atmos. Sci., 41, 402-413.

Randall, D. A., 1984b: Stratocumulus cloud deepening through entrainment. Tellus, 35A, (to appear).

Randall, D. A., J. A. Abeles, and T. G. Corsetti, 1985: Seasonal simulation of the planetary boundary layer and boundary-layer stratocumulus clouds with a general circulation model. Submitted to J. Atmos. Sci.

Rasmusson, E. M., 1967: Atmospheric water vapor transport and the hydrology of North America: Part I, Characteristics of the water vapor flux field. Mon. Wea. Rev., 95, 403-426.

Rasmusson, E. M., 1968: Atmospheric water vapor transport and the water balance of North America: Part II, Large-scale water balance investigations. Mon. Wea. Rev., 96, 720-734.

Rodgers, C. D., 1968: Some extensions and applications of the new random model for molecular band transmission. Quart. J. Roy. Met. Soc., 94, 99-102.

Schlesinger, Michael E., 1976: A numerical simulation of the general circulation of atmospheric ozone. PhD dissertation, UCLA, 375 pp.

Short, D. A., and J. M. Wallace, 1980: Satellite-inferred morning-to-evening cloudiness changes. Mon. Wea. Rev., 108, 1160-1169.

Shukla, J., D. Straus, D. A. Randall, Y. Sud, and L. Marx, 1982: Winter and summer simulations with the GLAS climate model. NASA Technical Memorandum 83866, 282 pp.

Slingo, J. M., 1982: A study of the earth's radiation budget using a general circulation model. Quart. J. R. Met. Soc., 108, 379-405.

Suarez, M. J., A. Arakawa, and D. A. Randall, 1983: The parameterization of the planetary boundary layer in the UCLA general circulation model: Formulation and results. Mon. Wea. Rev., 111, 2224-2243.

Susskind, J., J. Rosenfield, D. Reuter, and M. T. Chahine, 1984: Remote sensing of weather and climate parameters from HIRS2/MSU on TIROS-N. J. Geophys. Res., 89D, 4677-4698.

Stephens, G. L., G. G. Campbell, and T. H. Vonder Haar, 1981: Earth radiation budgets. J. Geophys. Res., 86c, 9739-9760.

Suarez, M. J., A. Arakawa, and D. A. Randall, 1983: The parameterization of the planetary boundary layer in the UCLA general circulation model: Formulation and results. Mon. Wea. Rev., 111, 2224-2243.

Vowinckel, E., and S. Orvig, 1970: The Climate of the North Polar Basin in World Survey of Climatology, Vol. 14, Climates of the Polar Regions. S. Orvig (ed.), New York: Elsevier, 370 pp.

Wetherald, R. T., and S. Manabe, 1980: Cloud cover and climate sensitivity. J. Atmos. Sci., 37, 1485-1510.